JOURNAL OF GEOPHYSICAL RESEARCH, VOL. 104, NO. C9, PAGES 20,837–20,856, SEPTEMBER 15, 1999

Arctic sea ice extents, areas, and trends, 1978-1996

Claire L. Parkinson, Donald J. Cavalieri, Per Gloersen, H. Jay Zwally, and Josefino C. Comiso

Oceans and Ice Branch, Laboratory for Hydrospheric Processes, NASA Goddard Space Flight Center Greenbelt, Maryland

Abstract. Satellite passive-microwave data for November 1978 through December 1996 reveal marked seasonal, regional, and interannual variabilities, with an overall decreasing trend of -34,300 ± 3700 km^2/yr (-2.8%/decade) in Arctic sea ice extents over the 18.2-year period. Decreases occur in all seasons and on a yearly average basis, although they are largest in spring and smallest in autumn. Regionally, the Kara and Barents Seas have the largest decreases, at -15,200 ± 1900 km^2/yr (-10.5%/decade), followed by the Seas of Okhotsk and Japan, the Arctic Ocean, Greenland Sea, Hudson Bay, and Canadian Archipelago. The yearly average trends for the total, the Kara and Barents Seas, and the Seas of Okhotsk and Japan all have high statistical significance, with the null hypothesis of a 0 slope being rejected at a 99% confidence level. Regions showing increasing yearly average ice extents are Baffin Bay/Labrador Sea, the Gulf of St. Lawrence, and the Bering Sea, with only the increases in the Gulf of St. Lawrence being statistically significant at the 99% level. Hemispheric results for sea ice areas exhibit the same -2.8%/decade decrease as for ice extents and hence a lower absolute decrease (-29,500 ± 3800 km^2/yr), with the ice-free area within the ice pack correspondingly decreasing at -4800 ± 1600 km^2/yr. Confidence levels for the trends in ice areas and ice-free water areas exceed 99% and 95%, respectively. Nonetheless, interannual variability is high, and, for instance, the Arctic Ocean ice extents have a positive trend 1990-1996, in spite of their negative trend for the time period as a whole.

1. Introduction

Sea ice is an integral component of the polar climate system [e.g., *Aagaard and Carmack*, 1989; *Barry et al.*, 1993], and its variability, seasonally, regionally, and interannually, has become increasingly quantified over recent decades as a result of a variety of in situ measurements, aircraft flights, submarine traverses, and especially satellite observations [e.g., *Pritchard*, 1980; *Parkinson et al.*, 1987; *Wadhams et al.*, 1991; *Parkinson and Cavalieri*, 1989; *Massom*, 1991; *Gloersen et al.*, 1992]. Important climatic roles of the ice include reflecting solar radiation away from the surface, serving as insulation between the atmosphere and the ocean, transporting relatively fresh surface water equatorward, and rejecting salt to the water underneath, thereby leading to densification of the water and, occasionally, to overturning. These roles, along with the vast expanse of the Arctic ice cover, ensure the importance of sea ice in the Arctic climate system. Major changes in Arctic climate will necessarily involve changes in the sea ice cover, as well as changes in other climate components, so that monitoring, reporting, and seeking to understand the ice variability are important aspects of seeking to understand polar climate and polar climate change.

Satellite passive-microwave observations provide the best data yet available for observing the full Arctic ice cover on a repetitive basis throughout the year. In this paper we report on the variability of the Arctic sea ice cover as determined from satellite passive-microwave data over the period from November 1978 through the end of 1996, which is the longest period so far with a compiled, quality-controlled satellite passive-microwave sea ice record in which data overlap exists for each change of satellite sensor. This work builds on and extends earlier studies of Arctic ice extents from the satellite passive-microwave record through mid-1987 [*Parkinson and Cavalieri*, 1989; *Gloersen and Campbell*, 1991] and through 1994/1995 [*Johannessen et al.*, 1995; *Maslanik et al.*, 1996; *Bjørgo et al.*, 1997], as discussed in sections 3 and 4. The new results show that the negative trends reported earlier for the Arctic ice cover as a whole have continued through 1996. The new results also add spatial and regional details, including trends in ice extent, ice area, and ice-free water area for each season in each of nine regions. Although 18.2 years is still inadequate for covering even one full solar cycle, it at least covers several El Niños and different stages of the North Atlantic Oscillation (NAO). While a much longer record is highly desired for long-term climate studies, the current results include negative yearly average ice extent trends statistically significant at a 99% confidence level or above in the Seas of Okhotsk and Japan, the Kara and Barents Seas, and the total, and a positive yearly average ice extent trend statistically significant at a 99% confidence level or above in the Gulf of St. Lawrence.

Paper number 1999JC900082.

2. Data

The data for this study come from the following four satellite instruments: the scanning multichannel microwave radiometer (SMMR) on board the Nimbus 7 satellite and the

special sensor microwave imagers (SSMIs) on board the Defense Meteorological Satellite Program's (DMSP's) F8, F11, and F13 satellites. The SMMR was operational on an every-other-day basis for most of the period from October 26, 1978, through August 20, 1987; the F8 SSMI was operational on a daily basis for most of the period from July 9, 1987, through December 18, 1991; the F11 SSMI was operational on a daily basis for most of the period from December 3, 1991, through September 30, 1995; and the F13 SSMI was operational on a daily basis for most of the period from May 3, 1995, through the end of December 1996.

Considerable effort has been expended to create from the four satellite data sets a unified passive-microwave sea ice concentration record for use in this and other sea ice studies. These efforts included eliminating bad data, interpolating for missing data, correcting for instrument drifts, intercalibrating the sensors using the periods of data overlap, adjusting the algorithm, and reducing false indications of sea ice resulting both from atmospheric weather conditions and from land-to-ocean spillover in the vicinity of coastal boundaries. All of these corrections are detailed by *Cavalieri et al.* [1999]. The result is a record including data throughout most of the north polar region (everywhere south of 84.6°N) every other day from October 26, 1978, through August 20, 1987, and daily from July 9, 1987, through December 31, 1996, with the one major exception being a 6-week data gap from December 3, 1987, through January 12, 1988. The 6-week data gap was filled in by performing a multiple ordinary least squares regression at each grid point, incorporating the data from the 60 days preceding and the 60 days following the gap, as discussed in more detail by *Gloersen et al.* [this issue].

The ice concentration data are all mapped to a common grid placed on a polar stereographic projection with a grid cell size of 25 x 25 km [*National Snow and Ice Data Center (NSIDC)*, 1992]. Because of the satellite orbits and the instrument swath widths, the SMMR data do not extend poleward of 84.6° latitude and the SSMI data do not extend poleward of 87.6° latitude. To illustrate the grid, the ice concentration data, and the size of the 84.6°-90°N data hole, Plate 1a shows the average March and September results over the course of the 18.2-year record. March is generally the month of maximum ice coverage, and September is generally the month of minimum ice coverage.

The SMMR/SSMI-derived sea ice concentrations have been used to determine sea ice extents throughout the data record, with "ice extent" defined as the cumulative area of all grid cells (in the region of interest) having calculated sea ice concentrations of at least 15%. For our Arctic Ocean calculations, we assume that the region of missing data north of 84.6°N is fully covered by ice having concentrations of at least 15%, a safe assumption in view of the high ice concentrations generally surrounding the data hole (Plate 1a). While ice extent is the primary variable of analysis for this study, some results are also presented for two additional variables, the "ice area" and the "ice-free area within the ice pack." Ice area is the cumulative area of ice coverage, calculated as the sum, over pixels with ice concentration ≥15%, of the pixel area times the ice concentration. The ice-free area within the ice pack is the area of water uncovered by ice, calculated as the difference: ice extent – ice area. For the ice area calculations we assume full ice coverage, to 100%, north of 84.6°N. This is clearly a much more stringent and less safe assumption than the assumption of ≥15% ice coverage north of 84.6°N, used for the ice extent calculations. The only ice area curves affected are those for the Arctic Ocean and the total Northern Hemisphere (section 4, Figure 11). In both of those cases the curves are simply uniformly raised by 1.18 x 10^6 km^2 above where they would have been if we had instead removed the area of the central data hole from our calculations. Any trends or variability that might have occurred north of 84.6°N remain undisclosed by this data set.

3. Time Series of Sea Ice Extents

The variability of Arctic sea ice extents revealed by the satellite passive-microwave record from the SMMR and SSMI is presented here in the form of time series of monthly ice extents, monthly ice deviations, yearly ice extents, and seasonal ice extents. The monthly deviations are deviations from the 18- or 19-year average values for the particular month, and for that variable, the results for the Northern Hemisphere as a whole (although none of the individual regions) were previously reported by *Cavalieri et al.* [1997]. The full set of time series is presented first for the Northern Hemisphere's ice cover and then for the ice covers in each of the following nine regions: the Seas of Okhotsk and Japan, the Bering Sea, Hudson Bay, Baffin Bay/Labrador Sea, the Gulf of St. Lawrence, the Greenland Sea, the Kara and Barents Seas, the Arctic Ocean, and the Canadian Archipelago (Plate 1b). The "Northern Hemisphere" ice refers to the cumulative ice in the nine regions, meaning that the relatively small amount of sea ice outside of those regions is not included. In particular, ice in the Baltic Sea and the Gulf of Bothnia is not included, in large part owing to (1) the large percentage of ocean pixels that are near land and hence subject to contamination from the high microwave radiative emissions characteristic of land areas and (2) the low salt content in the Baltic Sea and the Gulf of Bothnia and the consequent possible inappropriateness of the sea ice algorithm tie points. Because of the large differences in the sizes of the regions and of the total, the y axis ranges used in the plots differ from region to region, requiring consideration of the scales as well as the heights of the curves when comparing the different plots.

Trends for the yearly and seasonal ice extents are calculated using linear least squares regression through the respective values for the 18 full years of the data set, 1979-1996. The slopes b of the least squares lines, $y = a + bx$, are tabulated in Table 1, along with their estimated standard deviations (or standard errors). Following *Draper and Smith* [1981] and *Taylor* [1997], in each case the estimated standard deviation is calculated as the square root of the estimated variance of b, i.e., as

$$\sqrt{\frac{n\sum(y_i - a - bx_i)^2}{(n-2)[n\sum x_i^2 - (\sum x_i)^2]}}$$

or, equivalently, as

$$\sqrt{\frac{n\sum y_i^2 - (\sum y_i)^2 - b^2[n\sum x_i^2 - (\sum x_i)^2]}{(n-2)[n\sum x_i^2 - (\sum x_i)^2]}}$$

The number of points n is 18, the number of years, and the summations are done from $i = 1$ through $i = n$. For each trend line a standard F test [*Pollard*, 1981] was performed, testing

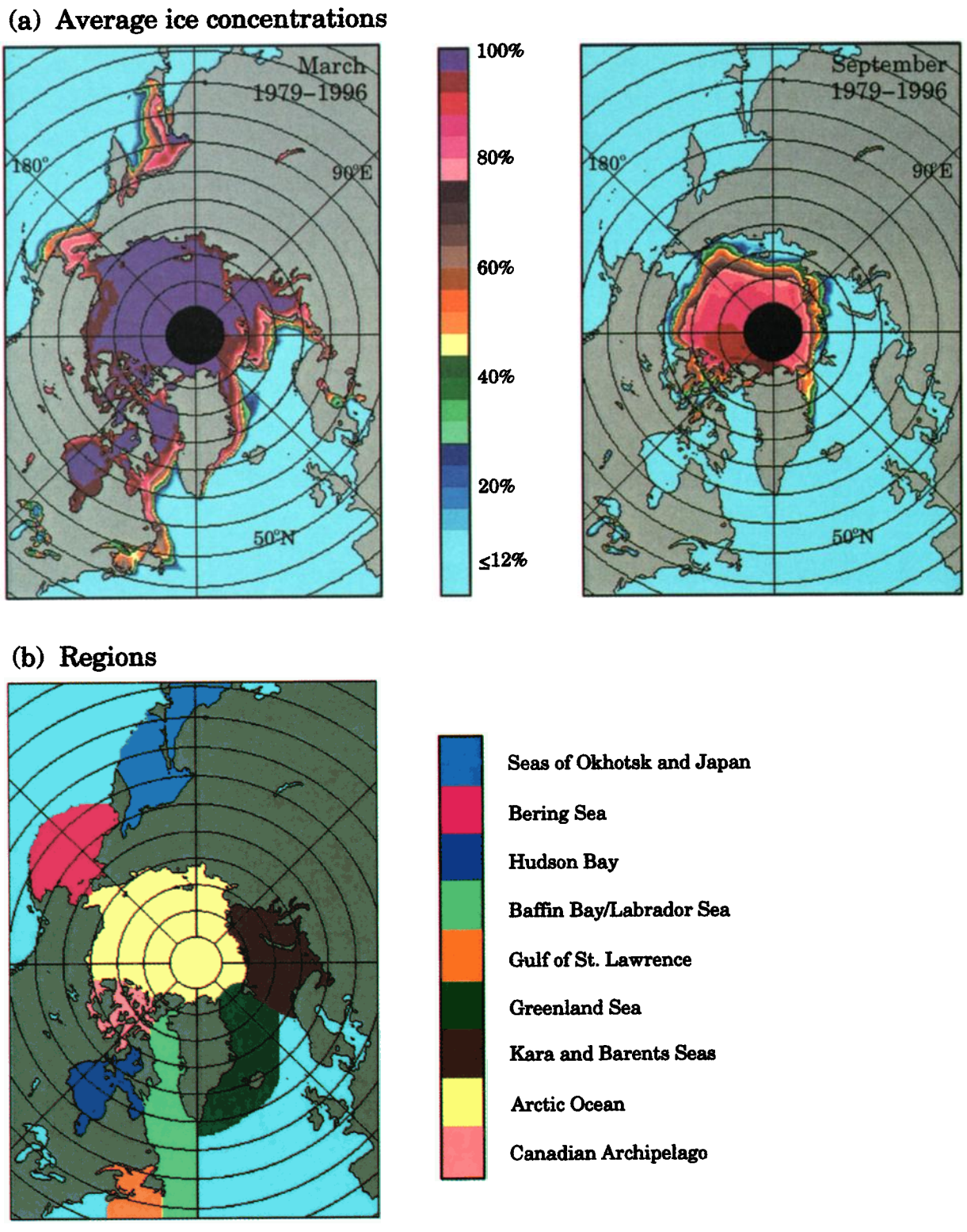

Plate 1. (a) Average March and September sea ice concentrations over the years 1979-1996, as calculated from the data of the Nimbus 7 SMMR and the DMSP F8, F11, and F13 SSMIs. (b) Location map of the regions used for analysis. The areas of the nine regions are: Seas of Okhotsk and Japan, 2.19 x 10^6 km^2; Bering Sea, 2.22 x 10^6 km^2; Hudson Bay, 1.22 x 10^6 km^2; Baffin Bay/Labrador Sea, 2.76 x 10^6 km^2; Gulf of St. Lawrence, 0.71 x 10^6 km^2; Greenland Sea, 2.91 x 10^6 km^2; Kara and Barents Seas, 2.58 x 10^6 km^2; Arctic Ocean, 7.08 x 10^6 km^2; and Canadian Archipelago, 0.74 x 10^6 km^2.

the null hypothesis of 0 slope, and all cases in which the null hypothesis can be rejected at confidence levels of 95% and 99% are identified as such in Table 1. For the F test, 16 degrees of freedom were used, two less than the number of years.

The data from the overlap periods were used to reduce inconsistencies between the data sets from the different instruments. The reader is referred to *Cavalieri et al.* [1999] for details on the procedures.

3.1. Northern Hemisphere

The average seasonal cycle of sea ice extents in the Northern Hemisphere has a minimum of 7.0 x 10^6 km^2 in September and a maximum of 15.4 x 10^6 km^2 in March (Figure 1a, inset). Growth is rapid and steady from September to December, then decelerates from December to March. The March-to-September decay period has maximum rates of decay occurring from June to August (Figure 1a, inset).

Interannually, the summer minima for the Northern Hemisphere ice extents exhibit greater variability than do the winter maxima (Figure 1a), but even the summer minima exhibit much less percent interannual variability than is found in several of the individual regions (sections 3.2 through 3.10), owing in part to compensating regional changes that are discussed in sections 3.2-3.10. Plotted monthly deviations (Figure 1b) show an overall negative trend in the Northern Hemisphere ice extents over the 18.2-year period, quantified in the $-34{,}300 \pm 3700$ km^2/yr slope of the linear least squares trend line (Figure 1b).

Yearly and seasonally averaged ice extents also all show negative trends for the Northern Hemisphere as a whole (Figure 1c, Table 1). Yearly ice extents had a high of 12.28 x 10^6 km^2 in 1982 and a low of 11.28 x 10^6 km^2 in 1995 (Figure 1c), with an overall trend of $-34{,}000 \pm 8300$ km^2/yr (Table 1). The seasonal slope of the largest magnitude ($-42{,}800 \pm 7500$ km^2/yr) is for the spring season; but the seasonal slope of the smallest magnitude, for autumn, is a substantial percentage (50%) of the spring slope (Figure 1c, Table 1). The autumn slope is not statistically significant at a 95% confidence level, while the others are, with the yearly, winter, and spring slopes all also being significant at a 99% confidence level (Table 1).

Our results correspond well with and extend to the end of 1996 several earlier findings of negative trends in the Arctic sea ice extents. Specifically, for the SMMR time period, October 1978 to August 1987, *Gloersen and Campbell* [1991] and *Johannessen et al.* [1995] obtain slopes of $-31{,}500$ and $-32{,}000$ km^2/yr, respectively. In an initial examination of the early portion of the SSMI data set, mid-1987 through the end of 1994, *Johannessen et al.* [1995] find a slope of $-54{,}000$ km^2/yr, suggesting an accelerated decrease. However, upon merging the SMMR and SSMI time series and extending the record through August 1995, they obtain the same $-32{,}000$ km^2/yr slope [*Bjørgo et al.*, 1997] that they had obtained earlier for the SMMR data [*Johannessen et al.*, 1995]. Our value of $-34{,}000$ km^2/yr (Table 1) for 1979-1996 is 6% greater, in absolute magnitude, than the *Bjørgo et al.* [1997] value through August 1995.

3.2. Seas of Okhotsk and Japan

The combined Seas of Okhotsk and Japan have a strong average seasonal cycle, with no ice cover during the summer months (July-September), only a slight ice cover during the

Table 1. Slopes of the Lines of Linear Least Squares Fit Through Yearly and Seasonal Arctic Sea Ice Extents, 1979-1996, With Estimated Standard Deviations for the 10^3 km^2/yr Values

Region	Yearly			Winter			Spring			Summer			Autumn		
	10^3 km^2/yr	S	%/dec	10^3 km^2/yr	S	%/dec	10^3 km^2/yr	S	%/dec	10^3 km^2/yr	S	%/dec	10^3 km^2/yr	S	%/dec
Northern Hemisphere	-34.0 ± 8.3	99	-2.8	-33.6 ± 9.2	99	-2.2	-42.8 ± 7.5	99	-3.1	-38.3 ± 17.6	95	-4.5	-21.5 ± 11.9		-1.9
Seas of Okhotsk and Japan	-9.7 ± 2.3	99	-20.1	-22.5 ± 6.3	99	-18.3	-14.5 ± 3.5	99	-27.2	0.0 ± 0.0		0.0	-2.0 ± 1.9		-11.0
Bering Sea	1.0 ± 1.7		3.3	3.5 ± 4.0		5.4	0.4 ± 3.6		1.0	-0.1 ± 0.0	99	-21.8	0.2 ± 1.8		1.2
Hudson Bay	-1.4 ± 1.4		-1.8	-0.0 ± 0.0		-0.0	-1.4 ± 0.8		-1.2	-1.4 ± 2.9		-5.4	-2.9 ± 3.6		-4.7
Baffin Bay/Labrador Sea	3.1 ± 3.8		3.8	9.8 ± 7.5		7.5	2.2 ± 5.3		2.1	1.2 ± 2.8		4.7	-0.8 ± 3.7		-1.2
Gulf of St. Lawrence	2.0 ± 0.4	99	32.0	4.4 ± 1.3	99	24.9	2.5 ± 0.5	99	50.2	0.0 ± 0.0		0.0	1.3 ± 0.3	99	42.8
Greenland Sea	-4.5 ± 2.9		-6.1	-12.6 ± 4.7	95	-12.6	-3.2 ± 3.0		-3.8	-0.5 ± 3.8		-1.2	-1.7 ± 3.7		-2.6
Kara and Barents Seas	-15.2 ± 4.4	99	-10.5	-16.0 ± 4.9	99	-8.3	-25.9 ± 6.5	99	-13.8	-12.7 ± 6.5		-17.6	-6.1 ± 5.1		-4.8
Arctic Ocean	-8.7 ± 4.6		-1.3	-0.0 ± 0.2		-0.0	-2.3 ± 1.5		-0.3	-23.2 ± 13.0		-3.7	-9.2 ± 4.9		-1.3
Canadian Archipelago	-0.6 ± 0.7		-0.8	-0.0 ± 0.0		-0.0	-0.5 ± 0.3		-0.7	-1.4 ± 2.2		-2.4	-0.3 ± 0.6		-0.4

Values are given both as 10^3 km^2/yr and percent/decade. S indicates statistical significance and identifies those cases in which the null hypothesis of a 0 slope is rejected with a 95% confidence level (95) and a 99% confidence level (99), using a standard F test with 16 degrees of freedom.

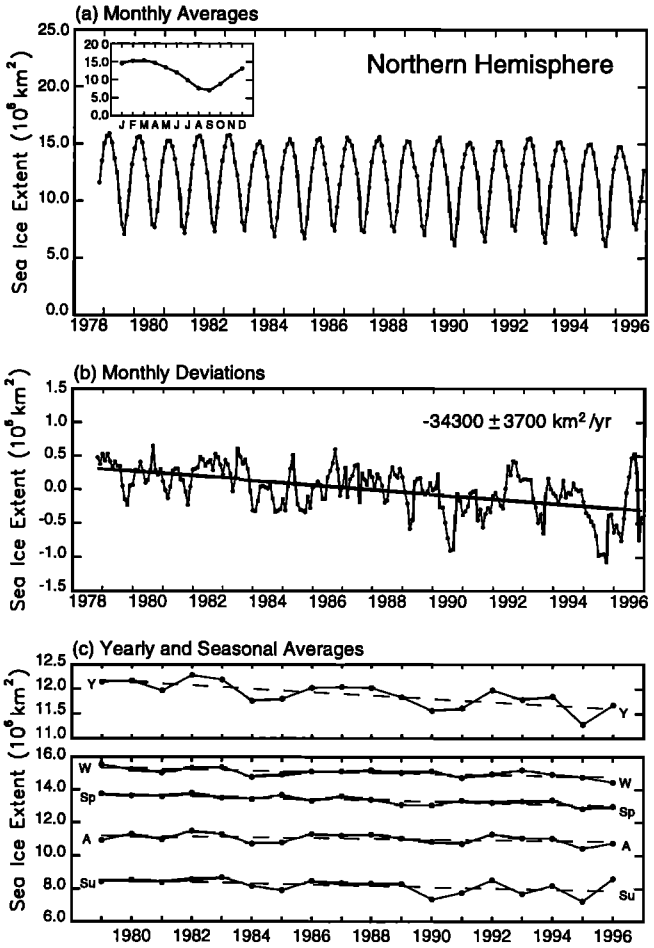

Figure 1. (a) Monthly averaged Northern Hemisphere sea ice extents from scanning multichannel microwave radiometer (SMMR) and special sensor microwave imager (SSMI) data, November 1978 through December 1996. The inset shows the average seasonal cycle over this time frame. (b) Monthly deviations for the Northern Hemisphere sea ice extents from SMMR and SSMI data, November 1978 through December 1996. The data for this plot were obtained by taking the monthly value for the individual month and subtracting the average value for that month over the 18.2-year period. Also shown is the line of linear least squares fit through the data and, at top right, the slope of that line and its estimated standard deviation. (c) Yearly and seasonally averaged Northern Hemisphere sea ice extents from SMMR and SSMI data, 1979-1996. Winter values (W) average the data for January-March, spring values (Sp) the data for April-June, summer values (Su) the data for July-September, and autumn values (A) the data for October-December.

autumn (October-December) and late spring (May-June), but a substantial ice cover in winter and early spring (January-April) (Figure 2a, inset). Growth is most rapid from December to January, and decay is most rapid from March to May (Figure 2a, inset).

The plotted monthly averages (Figure 2a), their deviations (Figure 2b), and the yearly averages (Figure 2c) all reveal a negative trend of sea ice coverage in the Seas of Okhotsk and Japan over the SMMR/SSMI period. In fact, the combined Seas of Okhotsk and Japan have one of the strongest indications of decreasing sea ice coverage of the nine Arctic regions, although because the summer ice always reaches 0 coverage, the visual impact of the decrease is somewhat dampened in the plot of monthly deviations (Figure 2b) versus the plots of monthly and yearly averages (Figures 2a and 2c). On a yearly average basis the first 2 years of the record have, by far, the greatest ice extents, and the 2 years with the lowest ice extents are both in the 1990s (Figure 2c). Overall, the downward slope of the yearly averages is 9700 ± 2300 km^2/yr, which converts to a substantial 20.1%/decade (Table 1), although not nearly as high a rate of decrease as was found for the Sea of Okhotsk during the SMMR years alone (see *Parkinson and Cavalieri* [1989], who found a slope of −22,000 km^2/yr).

On a seasonal basis the negative trend in ice extents in the Seas of Okhotsk and Japan is strongest in winter, with a linear least squares slope of −22,500 ± 6300 km^2/yr, and second strongest in spring, with a linear least squares slope of −14,500 ± 3500 km^2/yr (Figure 2c, Table 1). Summer ice extents show no interannual variability and no trend (Figure 2c, Table 1) because of the ice cover's consistently decreasing to 0 at that time of year (Figure 2a).

Interannual variability in the winter ice extents of the Seas of Okhotsk and Japan is substantial (Figure 2a). The year 1984 stands out in particular as having an anomalously low

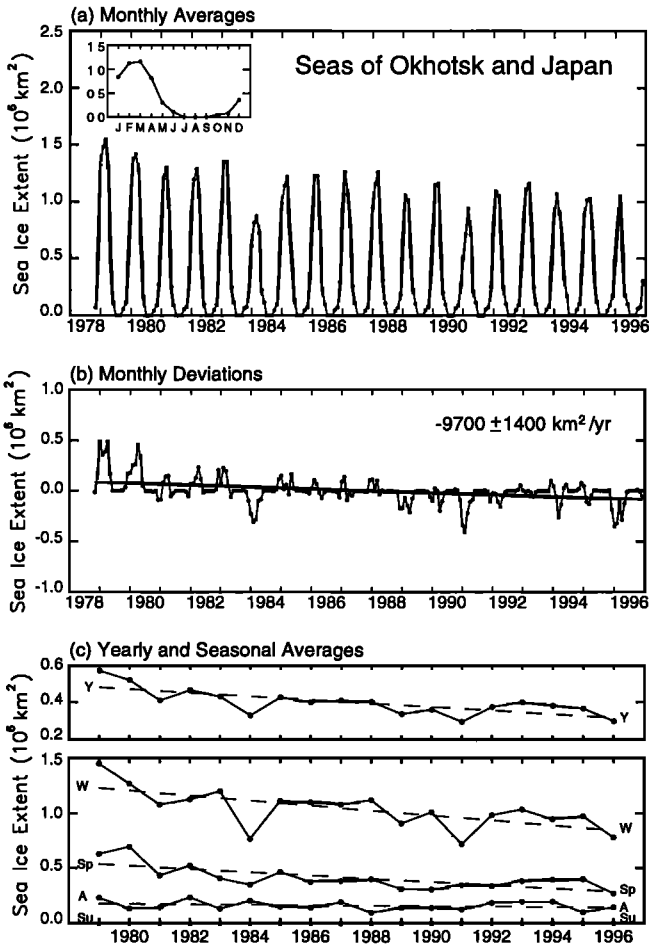

Figure 2. Same as for Figure 1, except for the Seas of Okhotsk and Japan.

wintertime ice coverage, with its month of maximum ice coverage (March) having the lowest maximum ice extent in the 18.2-year record and all 3 of its winter months having ice extents well below those of the preceding and succeeding years (Figure 2a). A possible explanation for the low 1984 ice extents is the dominance of the Aleutian Low pressure system over the Sea of Okhotsk in January-March of that year [*Parkinson*, 1990], with air flow coming largely from the Bering Sea instead of from the colder Siberian region, as would occur when the air flow over the Sea of Okhotsk is dominated by the Siberian High. January and February 1991 also stand out as having low ice coverages, although in that year the monthly average ice cover grew substantially from February to March (Figure 2a). Still, the January and February ice extents are sufficiently low that the overall winter ice extents in 1991 are even lower than those in 1984 (Figure 2c).

3.3. Bering Sea

The Bering Sea, located on the opposite side of Kamchatka Peninsula from the Sea of Okhotsk, is similar to the Seas of Okhotsk and Japan in terms of being a seasonal sea ice zone with ice coverage reducing to 0 in late summer. However, the Bering Sea has some out-of-phase aspects with respect to the Sea of Okhotsk [e.g., *Cavalieri and Parkinson*, 1987], resulting in quite different trends. More specifically, the year with the lowest maximum ice extents in the Sea of Okhotsk, 1984, has high maximum ice extents in the Bering Sea, and the year with the highest maximum ice extents in the Sea of Okhotsk, 1979, has low maximum ice extents in the Bering Sea (Figures 2a and 3a). The existence of some years with an out-of-phase aspect between the two seas is not surprising, as a persistent Aleutian Low, appropriately linked with a Siberian High to the west, can, depending on its positioning, result in opposite responses in the two seas. For instance, a prominent Aleutian Low positioned just east of Kamchatka Peninsula, with a strong Siberian High in far eastern Siberia, would encourage low ice coverages in the Bering Sea, where the meridional wind forcing would be from the south, and high ice coverages in the Sea of Okhotsk, where the meridional wind forcing would be from the north. Additional discussion of the occasional out-of-phase nature of the ice covers in the Sea of Okhotsk and the Bering Sea is given by *Cavalieri and Parkinson* [1987].

On an average basis, the ice cover in the Bering Sea is typically negligible in July, August, and September and slight in October and November (Figure 3a, inset). The growth rates are greatest from November to January, then lessen from January to March, when the ice cover reaches its maximum extent. Decay proceeds slowly from March to April, then much more rapidly from April to June. The slight remaining ice cover in June is essentially gone in July (Figure 3a, inset).

Interannual variability in the Bering Sea ice extents is more apparent from the monthly averages (Figure 3a) than is any long-term trend, although a slight trend toward increasing ice extents exists (Figure 3a) and is quantified in the monthly deviations with a least squares slope of 1200 ± 1000 km^2/yr (Figure 3b) and in the yearly averages with a least squares slope of 1000 ± 1700 km^2/yr (Figure 3c, Table 1), with neither value being statistically significant at a 95% confidence level or above. The trend for yearly averages is only one fourth the 4000 km^2/yr yearly average trend found earlier for the SMMR years alone [*Parkinson and Cavalieri*, 1989]. In spite of the

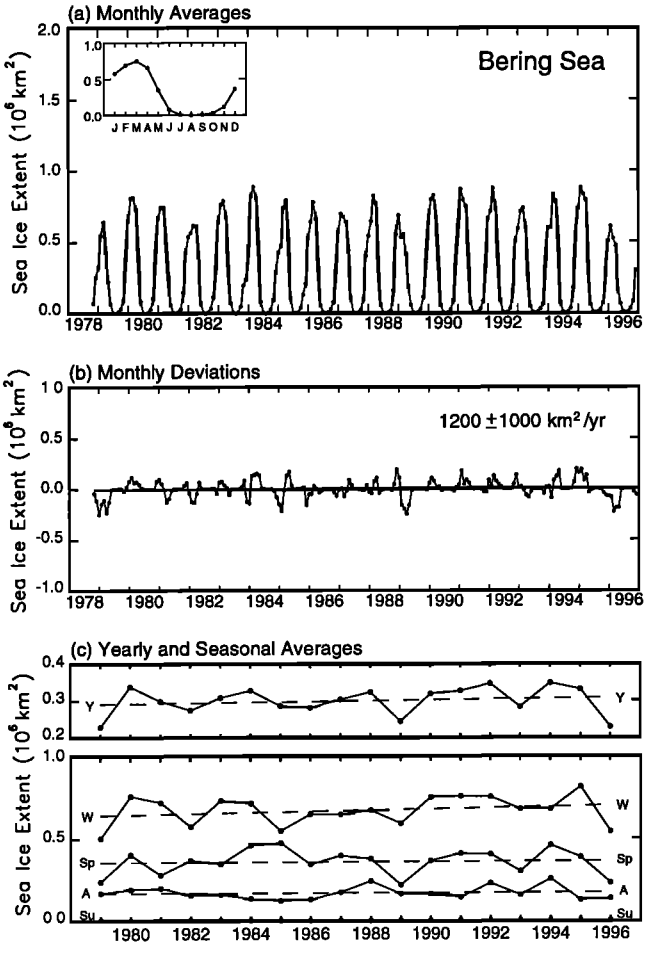

Figure 3. Same as for Figure 1, except for the Bering Sea.

overall positive trend, the lowest yearly average of the SMMR/SSMI data set came in the final year, 1996, with a value of 0.23 x 10^6 km^2 (Figure 3c). When viewed seasonally, the positive trend in Bering Sea ice extents is seen to derive predominantly from the behavior in the winter months (Figure 3c, Table 1).

3.4. Hudson Bay

In contrast to the Seas of Okhotsk and Japan and the Bering Sea, Hudson Bay is almost fully surrounded by land and has only relatively narrow passages linking it to the rest of the world's oceans (Plate 1b). This has marked impacts on the seasonal cycle of the Hudson Bay sea ice extents. Although its latitudinal range is comparable to those of the Sea of Okhotsk and the Bering Sea, its enclosed nature in the midst of the North American continent results in Hudson Bay's becoming fully ice covered through several months of the year. Full ice coverage (to at least 15% ice concentration in each pixel) lasted from January through April in all years of the data set and often included May as well (Figure 4a). On average over the 18.2 years, there was a slight decrease in ice extents from April to May, a greater decrease from May to June, and a much more rapid decay from June to August (Figure 4a, inset). Even in the months of minimum ice coverage, August-October, some ice remains, mostly in Foxe Basin, which is to the north of Hudson Bay proper but is

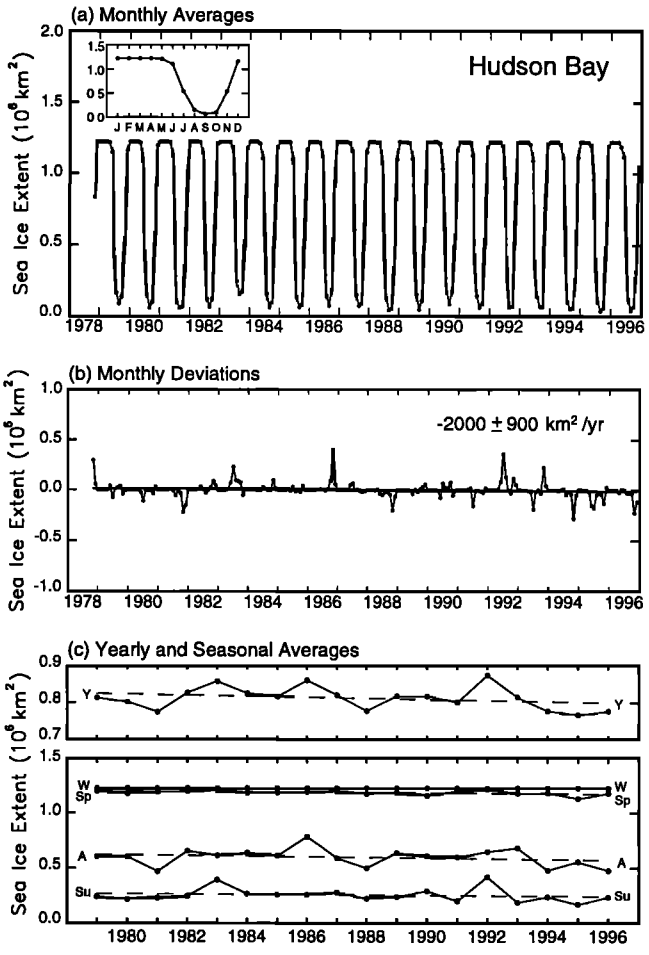

Figure 4. Same as for Figure 1, except for Hudson Bay.

included in the Hudson Bay region (Plate 1b). Growth is rapid from October through December, by which time the region is almost completely ice covered (to at least 15% ice concentration), so that the remaining growth from December to January is slight (Figure 4a, inset).

In view of the full ice coverage of Hudson Bay during each winter of the data set, interannual variability in this region is much less noticeable than in either of the previous two regions (Figure 4a versus Figures 2a and 3a). However, variability is apparent in summer and autumn (Figures 4a and 4c), and when monthly deviations are plotted, particular months stand out as having noticeable deviations, most prominently the unusually heavy November ice coverage in 1986 (Figure 4b). Overall, the monthly deviations show a slight negative trend, with a slope of -2000 ± 900 km^2/yr (Figure 4b). The negative trend is apparent also in the yearly averages (Figure 4c), although in spite of the negative trend, the year with the greatest yearly averaged ice extent came fairly late in the record, in 1992 (Figure 4c). This negative trend for 1979-1996 is reversed from the 10,000 km^2/yr positive trend earlier found for the SMMR years alone [*Parkinson and Cavalieri*, 1989].

Viewed seasonally, the negative trend in Hudson Bay ice extents is seen to derive mostly from the autumn conditions, although also somewhat from the spring and summer (Figure 4c, Table 1). This contrasts with the negative trend in the Seas of Okhotsk and Japan, which derives mostly from the winter and spring seasons (Figure 2, Table 1). The heavy yearly average ice coverage in Hudson Bay in 1992 (Figure 4c) is predominantly due to the late ice retreat in 1992 (Figure 4c), when 74% of the bay continued to have ice concentrations exceeding 15% in July (Figure 4a). This year was both preceded and followed by years with July ice (≥ 15% concentration) covering less than 32% of the region (Figure 4a).

3.5. Baffin Bay/Labrador Sea

Unlike Hudson Bay, the Baffin Bay/Labrador Sea region has a major opening to the North Atlantic and considerable exchange of waters with that ocean (Plate 1b). Furthermore, it is never ice covered throughout the region and hence has much greater wintertime interannual variability than does Hudson Bay, which typically is completely ice covered (to an ice concentration of at least 15%) for much of the winter season. Over the SMMR/SSMI time period, Baffin Bay/Labrador Sea ice extents experienced an average seasonal cycle ranging from minimum values of 0.09 x 10^6 km^2 in September to maximum values of 1.45 x 10^6 km^2 in March (Figure 5a, inset). Both the growth and decay periods are more uniformly paced (Figure 5a) than in any of the other regions. On an average basis the growth rate is modest from September to

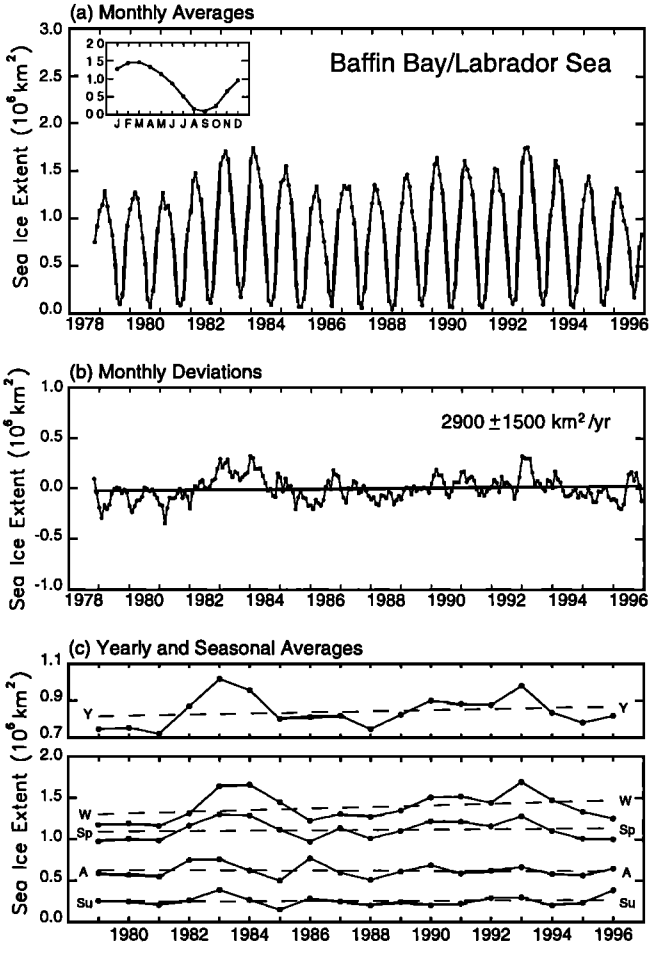

Figure 5. Same as for Figure 1, except for Baffin Bay/Labrador Sea.

October, is at its maximum from October to November, then gradually slows over the period from November to March (Figure 5a, inset). Decay begins from March to April, gradually increases until reaching its maximum values from June to August, then slows considerably from August to September (Figure 5a, inset).

Maximum ice extents in Baffin Bay/Labrador Sea exhibit cyclical behavior over the 18.2-year record, with low values in 1979-1981, high values in 1983-1984, low values in 1986-1988, high values in 1990 and 1993, and decreases in the final years of the data set (Figure 5a). This cyclical nature is discussed in more detail by *Parkinson* [1995], and the high values in 1983 and 1984 are tied to the century's then strongest El Niño-Southern Oscillation (ENSO) event, in 1982/1983, by *Mysak et al.* [1996]. *Mysak et al.* [1996] also note that anomalously large ice coverages tend to occur in the Labrador Sea about every 10 years and that these are associated with anomalously low air and ocean temperatures.

The cyclical nature of the interannual variability in Baffin Bay/Labrador Sea ice extents dominates over any linear trends, although, overall, the ice extents experienced an increasing trend (Figures 5b and 5c; see also *Parkinson* [1995] and *Gloersen et al.* [1996]). On the basis of monthly deviations the slope of the line of linear least squares fit is 2900 ± 1500 km^2/yr (Figure 5b), while on a yearly average basis the linear least squares slope is a statistically insignificant 3100 ± 3800 km^2/yr (Figure 5c, Table 1). The trend values, however, are strongly dependent on the starting and ending times of the record, as would be the case with any strongly cyclical time series. For instance, if the record had started in 1983 instead of 1979, the trend of the yearly averages would have been negative, whereas if the record had started in 1979 but ended in 1993, the trend would have been much more strongly positive than for the full 1979-1996 record (Figure 5c). Viewed seasonally, the positive overall slope derives predominantly from the winter season, which has a least squares slope over 3 times the yearly average slope (Figure 5c, Table 1). The spring and summer seasons have smaller positive slopes, while the autumn ice extents actually show a decreasing trend over the 18 years, although none of these slopes is statistically significant (Figure 5c, Table 1).

3.6. Gulf of St. Lawrence

The Gulf of St. Lawrence is the smallest and farthest equatorward of the nine regions (Plate 1b) and, relatedly, has the least ice coverage. Typically, ice extent in the Gulf of St. Lawrence is 0 in July, August, and September, rises very slightly from September to October, and increases much more from October to November (Figure 6a, inset). The growth rate slows from November to December, then speeds up from December through February. Decay proceeds from February through July, with the maximum decay rate occurring from March to April (Figure 6a, inset).

Ice extent in the Gulf of St. Lawrence reduces to 0 in each summer of the data set, while winter ice extents are generally lower in the first 6 years of the record than in the remaining years (Figure 6a). The result is that, even though the last 2 years show ice extent decreases (Figure 6a), the overall trends are toward increasing ice coverage over the 18.2-year record. This is true both of the monthly deviations (Figure 6b) and of the yearly averages (Figure 6c). Seasonally, the positive slope derives mostly from the winter season (Figure 6c), for which

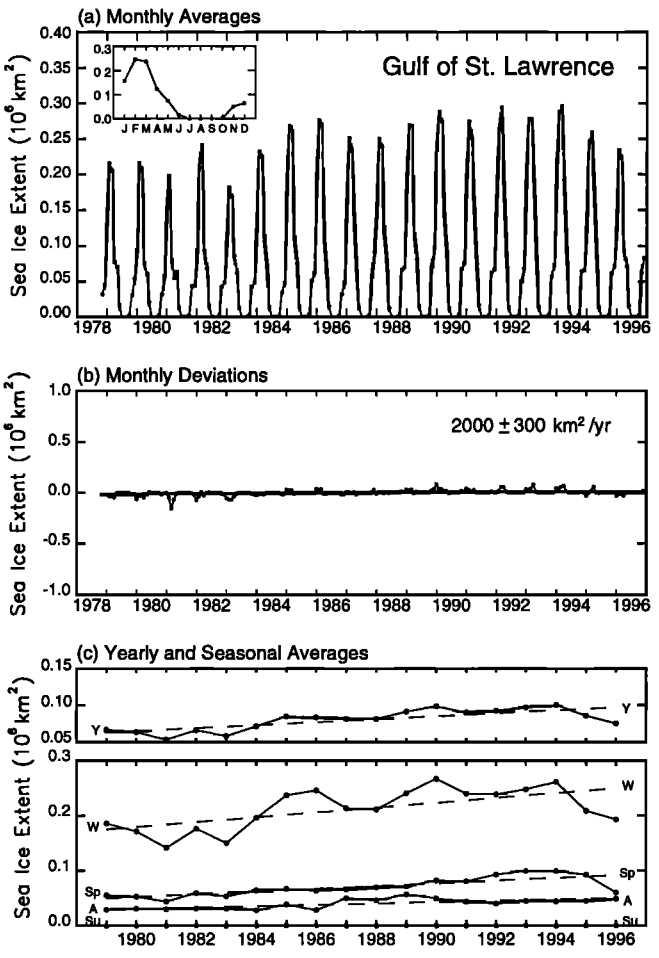

Figure 6. Same as for Figure 1, except for the Gulf of St. Lawrence.

the least squares slope exceeds twice that for the yearly averages (Table 1). The spring and autumn seasons also exhibit increasing ice coverage, while in the summer, when no ice exists, the trend is necessarily 0 (Figure 6c, Table 1).

The fact that both the Baffin Bay/Labrador Sea and Gulf of St. Lawrence yearly ice extents exhibit positive trends over the 18 years and that in both cases the positive slope derives mostly from the winter season is suggestive of a possible connection with larger-scale happenings in the northwestern North Atlantic. However, comparison of the monthly, yearly, and winter plots for the two regions (Figures 5 and 6) does not reveal a close correspondence between the fluctuations in the ice extents of the two regions. Hence the fact that both have positive slopes might not reflect a tight connection.

3.7. Greenland Sea

On an average basis the seasonal cycle of ice extents in the Greenland Sea ranges from a minimum of 0.35 x 10^6 km^2 in September to a maximum of 0.92 x 10^6 km^2 in March (Figure 7a, inset). However, the variability in the maximum and minimum ice extents is unusually high, with maximum values ranging from a low of 0.74 x 10^6 km^2 in 1994 to a high 50% higher (1.11 x 10^6 km^2) in 1979 and minimum values ranging from a low of 0.18 x 10^6 km^2 in 1985 to a high 150% higher (0.45 x 10^6 km^2) in 1995 (Figure 7a). The high variability

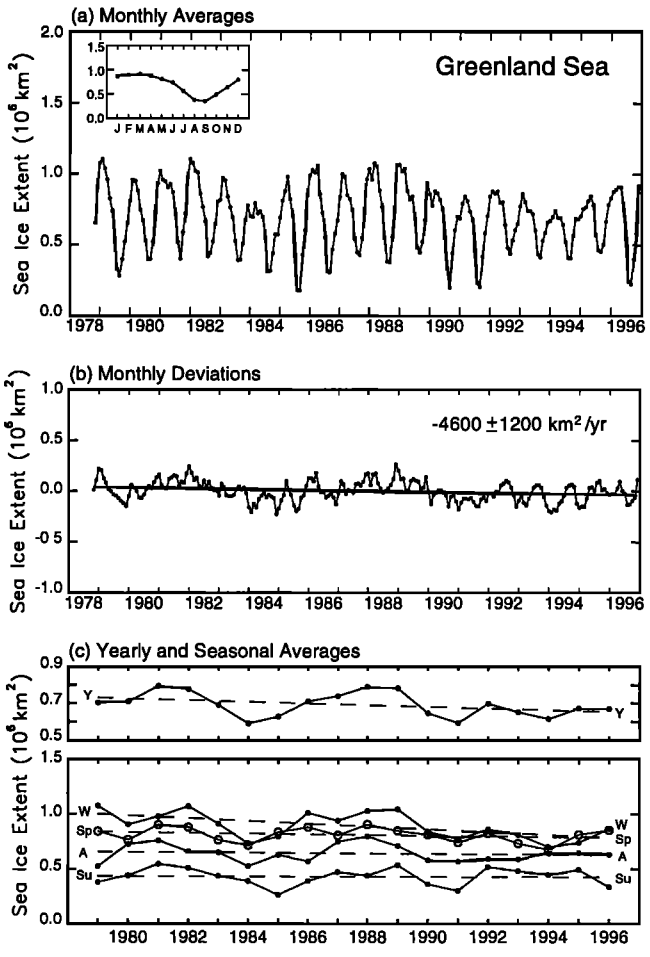

Figure 7. Same as for Figure 1, except for the Greenland Sea.

reflects the frequency, severity, and interannual variability in storm systems in this portion of the northern North Atlantic (see, e.g., *Serreze et al.* [1993] for a discussion of the synoptic activity).

Maximum ice extents in the Greenland Sea tend to be lower in the 1990s than in the earlier years of the data set, with the major exception coming with the low ice extents in 1984 (Figure 7a; see also *Gloersen et al.* [1992]). The amplitude of the seasonal cycle, however, is particularly small in 1992-1995, so that the minimum extents do not have the prominent downward trend of the maximum extents (Figure 7a). Still, the overall trends of both the monthly deviations and the yearly averages are negative, although with linear least squares slopes of only -4600 ± 1200 km^2/yr and -4500 ± 2900 km^2/yr, respectively (Figures 7b and 7c, Table 1). The negative trend for the yearly averages is reduced from the -8000 km^2/yr slope found for the SMMR years alone by *Parkinson and Cavalieri* [1989].

When examined seasonally, the negative trend in Greenland Sea ice extents is seen to exist in all seasons, although with a very slight magnitude in summer and by far the most substantial value, at $-12{,}600 \pm 4700$ km^2/yr, in winter (Figure 7c, Table 1). The winter slope is the only seasonal slope for the Greenland Sea with a statistical confidence level of 95% or above (Table 1). The Greenland Sea is unusual in having the averaged spring ice extents occasionally (1985 and 1995) exceed the averaged winter extents (Figure 7c), another peculiarity related to the storm systems over the northern North Atlantic [*Serreze et al.*, 1993]. Also, *Mysak and Power* [1992] attribute part of the variability in Greenland Sea ice coverage to variability in Mackenzie River runoff, with high runoffs being propagated as high ice cover anomalies from the Beaufort Sea to the Greenland-Iceland Sea, mentioning in particular the possible association of the high Greenland Sea ice extents in the late 1980s with earlier high Mackenzie runoffs. (See also *Häkkinen* [1993] for additional results on the propagation of anomalies into the Greenland Sea ice cover.)

Part of the variability in the Greenland Sea is due to the occurrence and non-occurrence of the "Odden," a large sea ice feature that occasionally exists in the east Greenland Sea between 73° and 77°N and sometimes protrudes eastward as far as 5°E. *Shuchman et al.* [1998] discuss the high variability of this feature and list its maximum area in each year 1978/1979 through 1993/1994. Of those years, the two weakest Oddens occurred in 1984 and 1994 [*Shuchman et al.*, 1998], the 2 years with the lowest Greenland Sea winter ice extents in Figures 7a and 7c. Even at its maximum, however, in 1986, the area of the Odden is only 289,181 km^2 [*Shuchman et al.*, 1998], which is less than a third of the average winter area of the Greenland Sea ice cover (Figure 7c). Hence

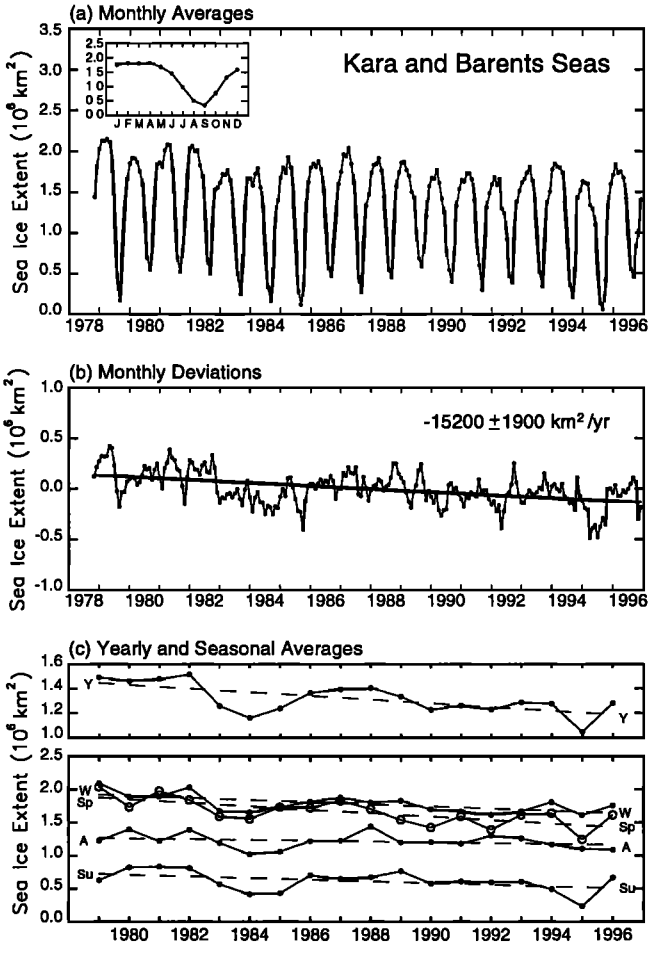

Figure 8. Same as for Figure 1, except for the Kara and Barents Seas.

it is not surprising that the area of the Odden [*Shuchman et al.*, 1998] and the area of the Greenland Sea ice coverage (Figure 7) do not track each other precisely. In an effort to explain the variability of the Odden, *Shuchman et al.* [1998] compare the satellite passive-microwave Odden observations with meteorological data from the International Arctic Buoy Program (IABP), finding that the meteorological parameters of most importance to the formation and decay of the Odden are, in order, air temperature, wind speed, and wind direction. Relatedly, in a case study of the 1995/1996 Odden, *Toudal Pedersen et al.* [1997] find the short-term development of the Odden to be closely correlated with local temperature and wind conditions.

3.8. Kara and Barents Seas

On an average basis, monthly sea ice extents in the Kara and Barents Seas reach a minimum in September and increase rapidly from September to November (Figure 8a, inset). Increases continue, although at a much smaller rate, until maximum ice extents are reached in April. The April-September decay has maximum rates from June to August (Figure 8a, inset).

Like the Greenland Sea, the Kara and Barents Seas region shows considerable interannual variability in its minimum monthly average ice extent, ranging from a low of 0.057 x 10^6 km^2 in 1995 to a high an order of magnitude larger, at 0.587 x

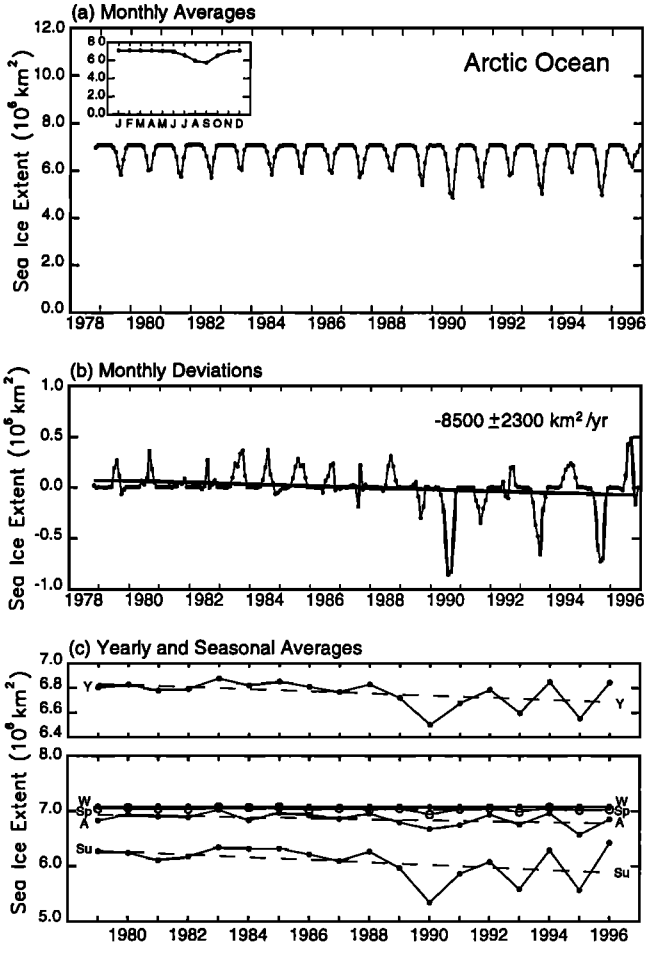

Figure 9. Same as for Figure 1, except for the Arctic Ocean.

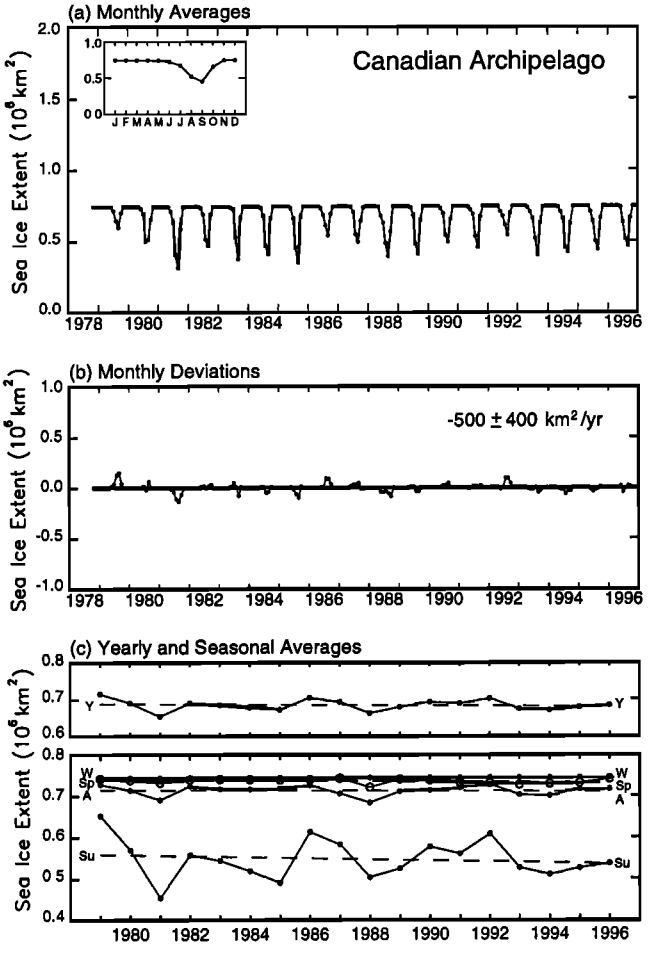

Figure 10. Same as for Figure 1, except for the Canadian Archipelago.

10^6 km^2, in 1989 (Figure 8a). Percentagewise, the variability in ice extent maxima is considerably less, with values ranging from a high of 2.15 x 10^6 km^2 at the start of the data set, in 1979, to a low of 1.63 x 10^6 km^2 near the end of the data set, in 1995 (Figure 8a). The overall trend in ice extent maxima is clearly negative over the course of the 18-year record (Figure 8a), while the minimum values reveal more of a highly variable behavior than a long-term trend (Figure 8a).

Overall, the monthly deviations for the Kara and Barents Seas have a downward trend with a slope of −15,200 ± 1900 km^2/yr (Figure 8b) and the yearly averages have a downward trend with a slope of −15,200 ± 4400 km^2/yr (Figure 8c, Table 1). The negative trend in yearly ice extents in the Kara and Barents Seas is statistically significant at a 99% confidence level and has the highest magnitude of any of the nine regions, contributing the most to the negative trend in the hemispheric values (Table 1). Nonetheless, this negative trend has a lower magnitude than the −32,000 km^2/yr slope found for the SMMR years alone [*Parkinson and Cavalieri*, 1989], suggesting that the decreases at least are not accelerating.

When examined seasonally, ice extents in the Kara and Barents Seas exhibit decreases in each of the four seasons, and the winter decreases apparent from the plot of monthly averages (Figure 8a) are seen to be exceeded by the spring decreases (Figure 8c, Table 1). The spring decreases in the Kara and Barents Seas are significant enough to stand out

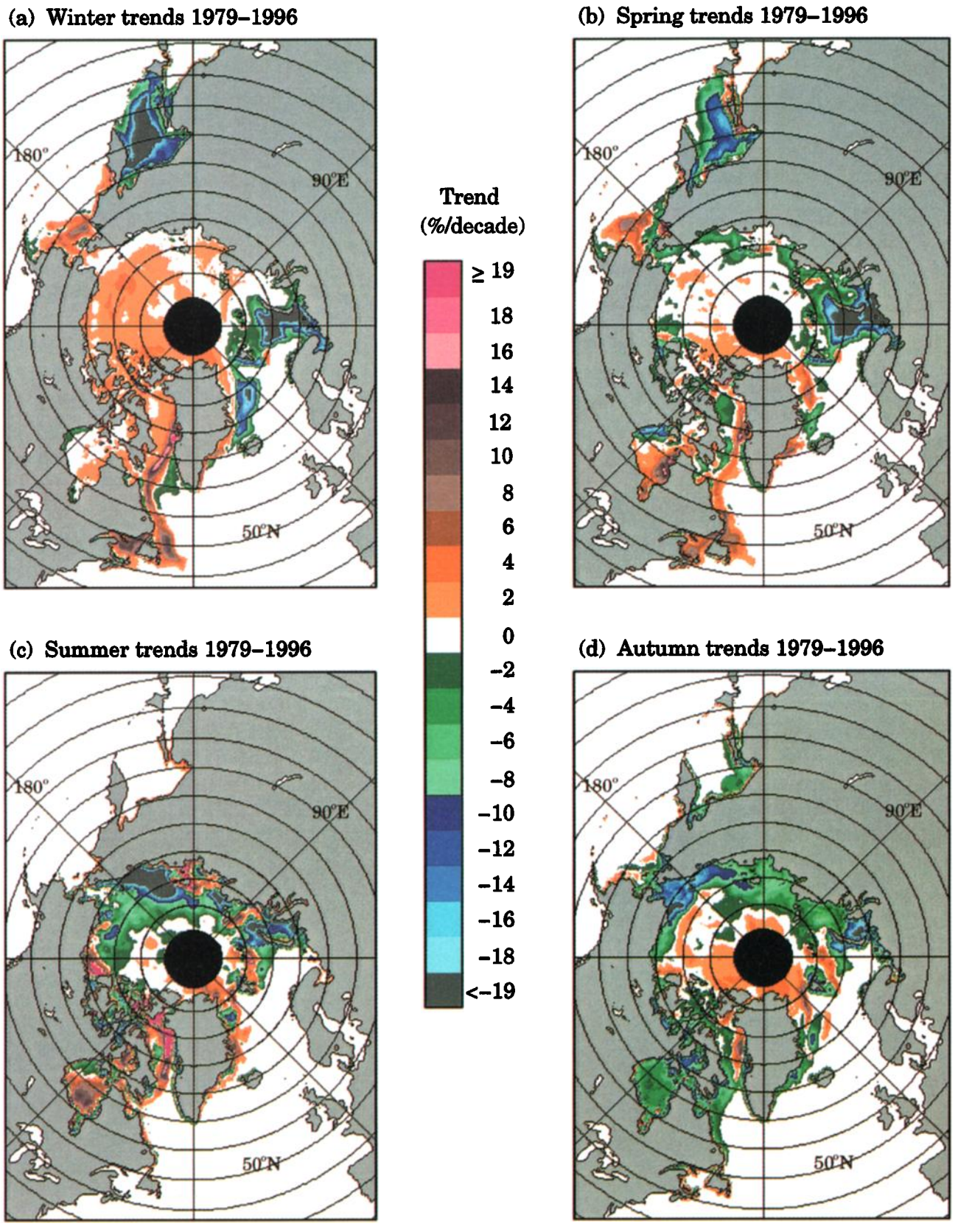

Plate 2. Decadal trends in the north polar seasonal sea ice concentrations over the period 1979-1996 for (a) winter, (b) spring, (c) summer, and (d) autumn. The trends were calculated from the daily sea ice concentrations by multiple ordinary least squares regression on a pixel-by-pixel basis after removal of the seasonal cycle.

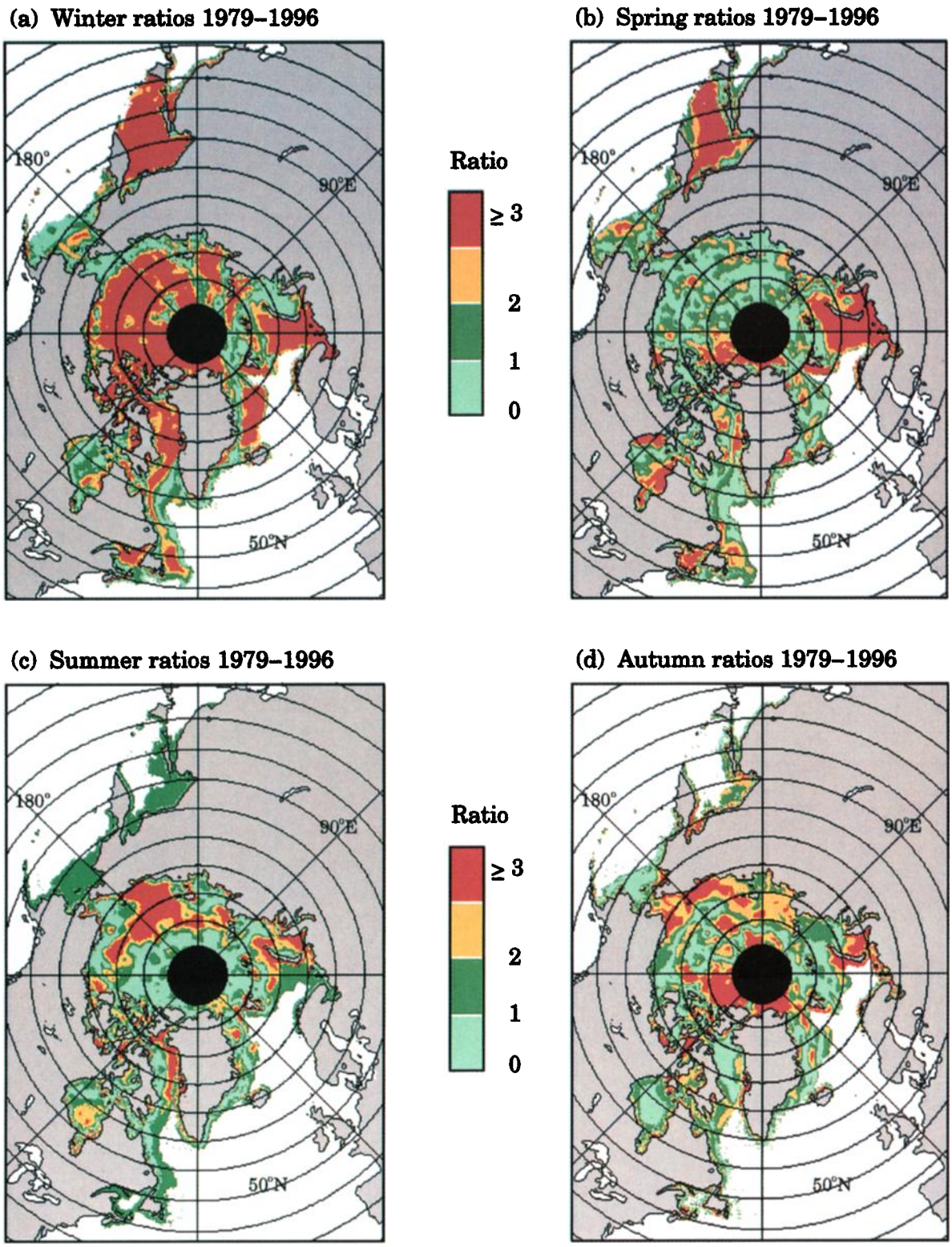

Plate 3. Ratio of the decadal trends in sea ice concentrations (Plate 2) to their estimated standard deviations, calculated on a pixel-by-pixel basis for (a) winter, (b) spring, (c) summer, and (d) autumn.

regionally as well, being 78% higher than the spring decreases in the Seas of Okhotsk and Japan and more than 8 times the magnitude of the spring decreases in any of the other regions (Table 1).

3.9. Arctic Ocean

The Arctic Ocean is fully ice covered (to at least 15% ice concentration) in at least 1 month of each year and generally for at least 3 months, most typically, February-April (Figure 9a). The average seasonal cycle shows near full ice coverage from December through April, followed by a slight opening in May and more marked declines from May through September (Figure 9a, inset). Ice growth in autumn is more rapid than the decay, being complete in the 3 months from September to December. The most rapid growth, on a monthly basis, is at the start of the growth period, from September to October, whereas the most rapid decay is late in the decay period, from July to August (Figure 9a, inset).

Overall trends in the minimum ice extent are clearly negative over the course of the data set (Figure 9a), as is reflected in the strongly negative slope in the summertime linear least squares fit (Figure 9c, Table 1). The monthly deviations and yearly averages show more clearly the negative slope for the record as a whole, while also highlighting the greatly increased variability in the 1990s versus that in the earlier years of the record (Figures 9b and 9c). The negative slope in the yearly averages (Table 1) is reversed from the slight, 5000 km^2/yr, positive slope found for the SMMR years alone [*Parkinson and Cavalieri*, 1989].

Seasonally, summer not only contributes the most to the negative trend of the yearly averages (Figure 9c, Table 1) but also is the season with the most obvious increase of variability in the 1990s (Figure 9c). Smaller but still clearly negative trends exist also in the spring and autumn ice extents, while trends in the winter, which consistently has nearly full ice coverage, are near 0 (Figure 9c, Table 1).

In spite of the negative slopes of the trend lines over the 1979-1996 period, the final year of the record has high summer and high yearly ice extents and, in fact, has the highest average summer ice extent of the entire record (Figures 9a, 9b, and 9c). Furthermore, both the yearly average and the summer seasonal average ice extents have their lowest values in 1990, and both variables show upward trends during the 1990s (Figure 9c). The particularly low summer minimum ice extents in the Arctic in 1990 are analyzed by *Serreze et al.* [1995], where they are put in the broader context of a geographically larger-scale warm atmospheric temperature anomaly in spring and summer 1990 and a record minima in snow coverage over the Eurasian landmass from February through September 1990 [*Robinson et al.*, 1993].

Maslanik et al. [1996] examine SMMR/SSMI time series for November 1978 to September 1995 for a region covering the Arctic Ocean, the Kara Sea, the Barents Sea, and the northern portion of the Greenland Sea. They obtain a trend of –25,000 km^2/yr, which is between the –23,900 km^2/yr sum of the yearly values in Table 1 for the Arctic Ocean and the Kara and Barents Seas, and the –28,400 km^2/yr sum of the Table 1 yearly values for the Arctic Ocean, the Kara and Barents Seas, and the Greenland Sea, showing a good correspondence between the results through September 1995 [*Maslanik et al.*, 1996] and those through December 1996 (Table 1). Also, as in Table 1, *Maslanik et al.* [1996] find the decreases to be greatest in summer, which in their case is an expanded summer season lasting from May through September.

3.10. Canadian Archipelago

The Canadian Archipelago has an average seasonal cycle very similar in shape to that of the Arctic Ocean, with near full ice coverage (to at least 15% ice concentration) from December through April, most rapid decay from July to August, minimum ice extent in September, and most rapid growth from September to October (Figure 10a, inset). Differences include the much smaller area involved in the Canadian Archipelago and the fact that in the case of the archipelago, November has very close to full ice coverage also (Figure 10a, inset versus Figure 9a, inset).

Ice extents in the Canadian Archipelago remain within 0.1% of their maximum possible, the full areal extent of the archipelago, for several months in each year, lasting from November through May in the majority of the years. The exceptions to the November-May duration of maximum ice coverage all involve shortened durations. Specifically, in 1980/1981, 1990/1991, 1991/1992, and 1992/1993, maximum ice coverage started in November but only lasted through April; in 1981/1982, 1993/1994, and 1994/1995, maximum ice coverage started in December, ending in April in 1994 and 1995 but in May in 1982; and in 1987/1988, the year with the shortest period of maximum ice coverage, maximum ice coverage lasted from December to March (Figure 10a).

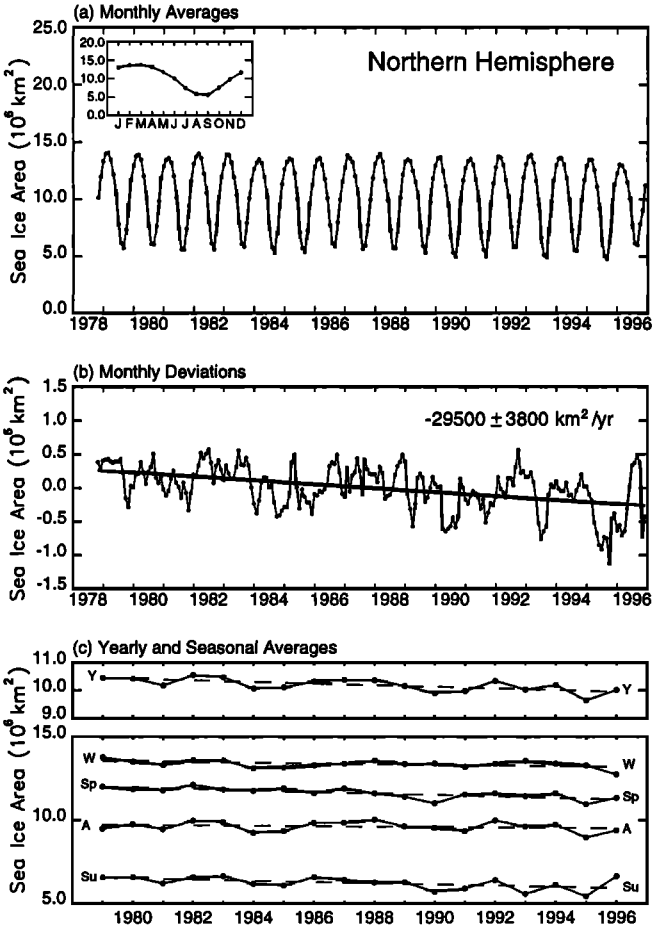

Figure 11. Same as for Figure 1, except for sea ice areas instead of sea ice extents.

Long-term trends for the ice extents in the Canadian Archipelago over the SMMR/SSMI period are nearly imperceptible, as they are also for the SMMR years alone [*Parkinson and Cavalieri*, 1989]. Quantitatively, the slope of the least squares trend line is -500 ± 400 km^2/yr for the monthly deviations (Figure 10b) and a statistically very insignificant -600 ± 700 km^2/yr for the yearly averages (Figure 10c, Table 1). Seasonally, the slopes are slightly negative, with the summer season having the slope of the largest magnitude, at -1400 ± 2200 km^2/yr, but with that too being statistically insignificant (Figure 10c, Table 1).

4. Ice Areas and Ice-Free Areas Within the Ice Pack

Examination of ice areas (cumulative sums, over a region, of pixel area times ice concentration) reveals strong qualitative similarities with the ice extent results, although with the ice areas always lower than the ice extents (Figure 11 versus Figure 1). For the Northern Hemisphere as a whole, the ice areas, like the ice extents, show a 2.8%/decade decrease in the yearly values and decreases also in each of the four seasons, with the largest seasonal percent/decade decrease coming in summer (Tables 1 and 2). Plotted, the yearly and each of the seasonal ice area averages (Figure 11c) parallel quite closely the results for ice extents (Figure 1c), although with the percent/decade decreases being numerically larger for ice areas in spring and summer and for ice extents in autumn and winter (Tables 1 and 2), implying that, overall, the ice cover has become less compact (lower average ice concentration, calculated as area/extent) during spring and summer and more compact during autumn and winter.

Regionally, many of the numerical differences between the percent/decade trends for ice areas and ice extents are greater than the differences for the Northern Hemisphere as a whole, although the signs of the trends for each of the two sets of results are generally the same (Tables 1 and 2). In fact, the only cases (out of 45 regional and yearly/seasonal pairs of area and extent values) with differing signs are in Hudson Bay in winter, in Baffin Bay/Labrador Sea in autumn, in the Greenland Sea in autumn, in the Arctic Ocean in winter, and in the Canadian Archipelago in winter, in each of which the ice extents decreased while the ice areas increased, implying increased average ice concentrations, and in the Bering Sea in spring, in which case the ice extents increased while the ice areas decreased (Tables 1 and 2).

The ice-free areas within the ice pack follow very different seasonal patterns than the ice areas or ice extents. For instance, in regions such as the Arctic Ocean and the Canadian Archipelago, where most of the region is ice covered throughout the year, the ice-free area within the ice pack peaks in summer, when the ice concentrations are lowest, and has its lowest values in winter, when the ice concentrations are highest (Figures 12a and 12b). In contrast, in regions such as the Seas of Okhotsk and Japan and the Bering Sea, where the ice cover decreases to 0 or near 0 in summer but has no geographic barriers to southward expansion in winter, the seasonal cycle is similar to the cycles for ice areas and extents in terms of peaking in winter and decreasing to 0 in summer (Figures 12c and 12d). In still other regions the peak is typically in spring, one example being Hudson Bay, where the ice extent is very low in summer,

Table 2. Slopes of the Lines of Linear Least Squares Fit Through Yearly and Seasonal Arctic Sea Ice Areas, 1979-1996, With Estimated Standard Deviations for the 10^3 km^2/yr Values

Region	Yearly			Winter			Spring			Summer			Autumn		
	10^3 km^2/yr	S	%/dec	10^3 km^2/yr	S	%/dec	10^3 km^2/yr	S	%/dec	10^3 km^2/yr	S	%/dec	10^3 km^2/yr	S	%/dec
Northern Hemisphere	-29.3 ± 8.3	99	-2.8	-21.4 ± 9.6	95	-1.6	-45.9 ± 9.6	99	-3.8	-37.1 ± 14.9	95	-5.7	-13.0 ± 13.2		-1.3
Seas of Okhotsk and Japan	-9.1 ± 2.0	99	-27.4	-23.1 ± 5.7	99	-25.6	-11.7 ± 2.9	99	-34.0	0.0 ± 0.0		0.0	-1.9 ± 1.2		-21.1
Bering Sea	0.9 ± 1.3		5.1	3.6 ± 3.5		8.5	-0.1 ± 2.6		-0.3	-0.1 ± 0.0	99	-39.7	0.3 ± 1.4		3.3
Hudson Bay	-0.7 ± 1.3		-1.0	0.8 ± 0.6		0.7	-1.0 ± 1.5		-1.0	-0.4 ± 1.6		-3.8	-2.2 ± 3.6		-4.6
Baffin Bay/Labrador Sea	2.7 ± 3.2		4.3	9.8 ± 7.0		9.3	0.3 ± 4.1		0.3	0.3 ± 1.6		2.2	0.5 ± 3.2		1.2
Gulf of St. Lawrence	1.1 ± 0.3	99	33.3	3.1 ± 1.1	95	31.5	1.0 ± 0.3	99	46.2	0.0 ± 0.0		0.0	0.3 ± 0.1	99	24.6
Greenland Sea	-2.1 ± 2.3		-4.3	-7.3 ± 3.9		-10.4	-1.3 ± 2.1		-2.2	-0.4 ± 2.7		-1.9	0.4 ± 3.2		0.9
Kara and Barents Seas	-13.6 ± 4.0	99	-11.7	-16.8 ± 5.3	99	-10.0	-25.7 ± 6.3	99	-16.4	-7.6 ± 5.0		-17.7	-4.6 ± 4.9		-4.6
Arctic Ocean	-7.3 ± 4.9		-1.2	7.3 ± 1.9	99	1.1	-5.7 ± 3.8		-0.8	-25.2 ± 12.0		-4.8	-5.3 ± 7.0		-0.8
Canadian Archipelago	-1.2 ± 0.9		-2.0	1.3 ± 0.3	99	1.8	-1.9 ± 0.6	99	-2.7	-3.6 ± 2.4		-9.1	-0.6 ± 0.9		-1.0

S indicates statistical significance and identifies those cases in which the null hypothesis of a 0 slope is rejected with a 95% confidence level (95) and a 99% confidence level (99), using a standard F test with 16 degrees of freedom.

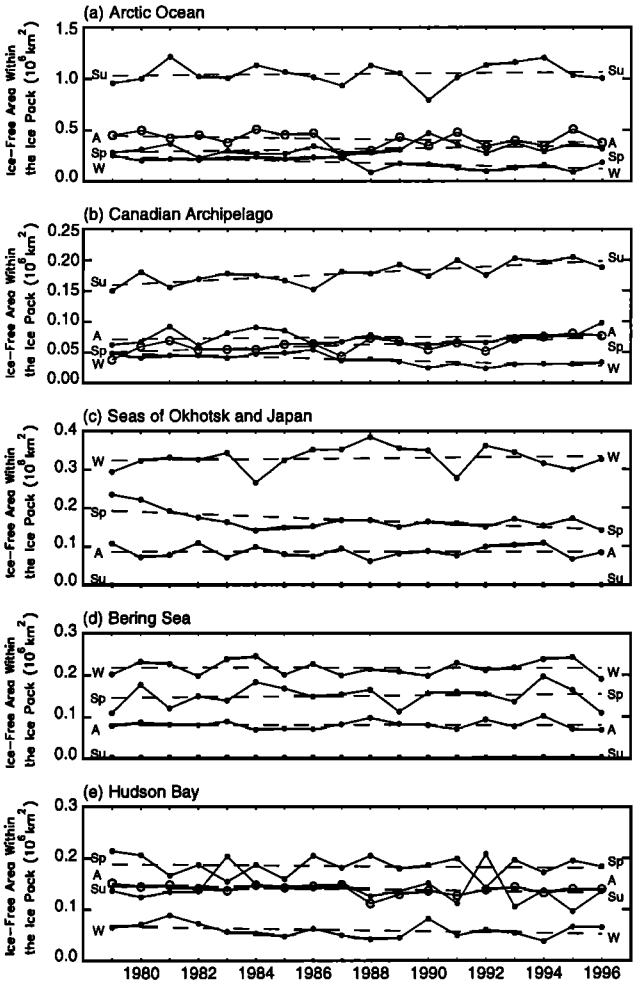

Figure 12. Seasonally averaged ice-free areas within the ice packs of the (a) Arctic Ocean, (b) Canadian Archipelago, (c) Seas of Okhotsk and Japan, (d) Bering Sea, and (e) Hudson Bay, from SMMR and SSMI data, 1979-1996. Winter values (W) average the data for January-March, spring values (Sp) the data for April-June, summer values (Su) the data for July-September, and autumn values (A) the data for October-December.

hindering a peaking then, and the ice concentration is very high in winter, hindering a peaking then (Figure 12e). Summing results for all the regions, ice-free areas within the ice pack for the Northern Hemisphere peaked in summer in all years except 1990 and 1995, when they peaked in spring (Figure 13c). The average seasonal cycle of ice-free areas within the ice pack shows a clear peak in July, with the June and August values also well above the values for the remainder of the year (Figure 13a, inset).

For the Northern Hemisphere as a whole, ice-free areas within the ice pack show decreases statistically significant at a 95% confidence level or above over the 1979-1996 period in the winter, autumn, and yearly averages, plus a statistically insignificant decrease in summer and a statistically insignificant increase in spring (Figure 13c, Table 3). The decreases in ice-free areas within the ice pack in winter and autumn follow from the fact that the ice extent decreases in those two seasons exceed the ice area decreases (Tables 1 and 2). Necessarily, in the five cases with decreasing ice extent but increasing ice area, enumerated in the second paragraph of this section, the ice-free area within the ice pack decreased (Table 3). Similarly, in the Bering Sea spring case, with increasing ice extent but decreasing ice area, the ice-free area within the ice pack necessarily increased (Table 3). Such a situation would be expected for regions experiencing increasing divergence of the ice cover.

Previous studies using a shorter period from the SMMR and/or SSMI records and examining the total north polar ice coverage also consistently report decreases in both the ice area and the ice-free area within the ice pack, although with a large range of magnitudes. For ice areas, *Gloersen et al.* [1992] and *Johannessen et al.* [1995] report slopes of –21,400 and –30,000 km^2/yr, respectively, for the SMMR years, *Johannessen et al.* [1995] report a slope of –49,000 km^2/yr for the SSMI years through the end of 1994, and *Bjørgo et al.* [1997] report a slope of –36,000 km^2/yr for the SMMR and SSMI years through August 1995. The slope of –29,300 ± 8300 km^2/yr for the Northern Hemisphere yearly values for 1979-1996 (Table 2) is within the wide range of the earlier reported values. Regarding ice-free areas within the ice pack, *Gloersen et al.* [1992] and *Johannessen et al.* [1995] report slopes of –10,200 and –1000 km^2/yr, respectively, for the

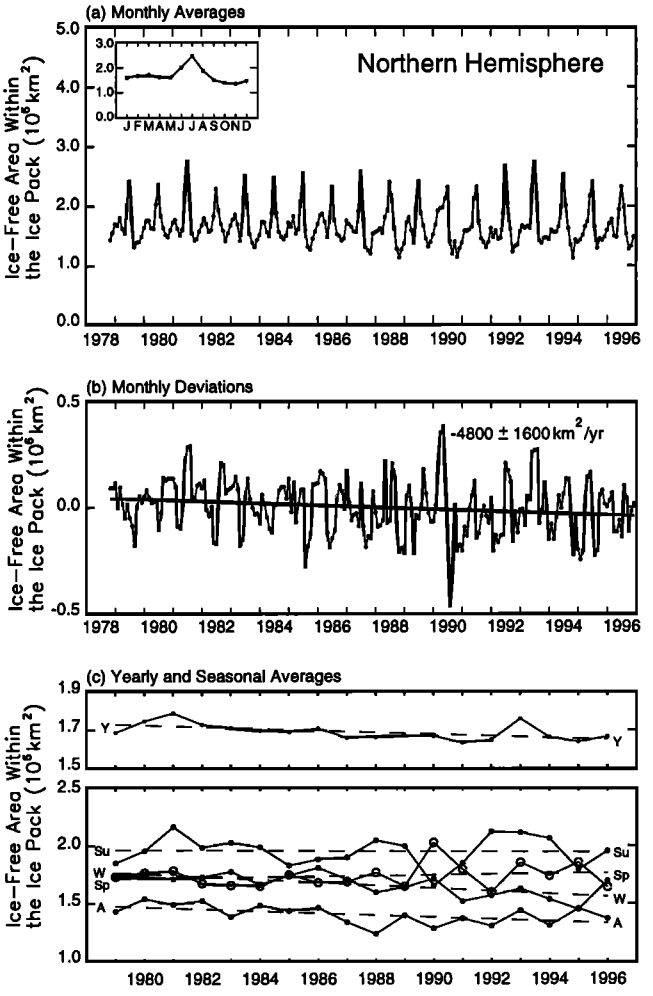

Figure 13. Same as for Figure 1, except for ice-free areas within the ice pack instead of sea ice extents.

SMMR years, and *Johannessen et al.* [1995] report a slope of –5000 km^2/yr for the SSMI years through the end of 1994. Once again, the new value (-4600 ± 1600 km^2/yr, Table 3) for 1979-1996 falls within the range of the previously reported values.

In both the current study and the previous ones a portion of the calculated ice-free area during summer is likely due to melt ponding on the ice and the failure of the passive-microwave algorithms to distinguish melt ponds from open water [*Gloersen et al.*, 1992; *Comiso and Kwok*, 1996]. More generally, calculated values of ice-free areas and ice areas are felt to have larger error bars during late spring and summer than during the rest of the year because of the complications caused by surface melt, freeze/thaw cycles, and ice decay, all affecting the ice emissivities [*Gloersen et al.*, 1992]. Quantitative comparisons of ice concentrations derived from passive-microwave and high-resolution synthetic aperture radar (SAR) data do show some marked differences in summertime [*Comiso and Kwok*, 1996], presumably caused in part by the surface melt and related complications.

5. Spatial Distributions of Trends

In the two preceding sections, the sea ice extents, sea ice areas, and ice-free areas within the ice pack were examined regionally and hemispherically. In this section, to present a more detailed spatial view, the 18-year seasonal sea ice concentration decadal trends are examined on a pixel-by-pixel basis. These trends have been calculated by multiple ordinary least squares regression from the every-other-day SMMR and SSMI data, as described by *Gloersen et al.* [this issue]. Estimated standard deviations of the trends are calculated following *Draper and Smith* [1981] after first removing the modeled seasonal cycle determined from the first five harmonics. The decadal trends in the Arctic winter (defined as January-March), spring (April-June), summer (July-September), and autumn (October-December) are shown in Plate 2, while the corresponding ratios of these values to their estimated standard deviations are shown in Plate 3. The larger the ratio, the greater is the statistical significance. Values outside the nine regions of interest (Plate 1b) and outside the maximum seasonal sea ice coverage within each region are not shown.

Examination of Plate 2 shows that the largest decadal trends, both positive and negative, in sea ice concentration occur within the seasonal sea ice zones. During winter the regions with the largest negative trends are in the central Sea of Okhotsk, the eastern Barents Sea, and the central Greenland Sea (Plate 2a). All these regions also show large ratios of trend to estimated standard deviation (Plate 3a), indicating a relatively large statistical significance. Large positive winter trends are found in a southwest/northeast stretch across Davis Strait and Baffin Bay, in the central part of the ice-covered area of the Labrador Sea, and throughout most of the ice-covered area of the Gulf of St. Lawrence (Plate 2a). In these areas as well, the trends are significant, with magnitudes exceeding 3 estimated standard deviations (Plate 3a). In the Sea of Okhotsk, where practically all of the pixels show wintertime ice concentration decreases (Plate 2a), it is understandable that the winter ice areas decreased (Table 2) and the ice-free areas within the ice pack increased (Table 3). In the Gulf of St. Lawrence, where most of the pixels

Table 3. Slopes of the Lines of Linear Least Squares Fit Through Yearly and Seasonal Arctic Ice-Free Areas Within the Ice Pack, 1979-1996, With Estimated Standard Deviations for the 10^3 km^2/yr Values

Region	Yearly			Winter			Spring			Summer			Autumn		
	10^3 km^2/yr	S	%/dec	10^3 km^2/yr	S	%/dec	10^3 km^2/yr	S	%/dec	10^3 km^2/yr	S	%/dec	10^3 km^2/yr	S	%/dec
Northern Hemisphere	-4.6 ± 1.6	95	-2.7	-12.2 ± 3.4	99	-6.9	3.2 ± 4.7		1.8	-1.2 ± 6.1		-0.6	-8.5 ± 3.4	95	-5.7
Seas of Okhotsk and Japan	-0.6 ± 0.4		-3.8	0.6 ± 1.4		1.9	-2.9 ± 1.0	99	-15.0	0.0 ± 0.0		0.0	-0.0 ± 0.7		-0.4
Bering Sea	0.0 ± 0.5		0.4	-0.1 ± 0.8		-0.5	0.4 ± 1.2		3.0	-0.0 ± 0.0	95	-12.4	-0.1 ± 0.5		-1.1
Hudson Bay	-0.8 ± 0.3	95	-5.5	-0.8 ± 0.6		-12.7	-0.5 ± 0.9		-2.5	-1.0 ± 1.3		-6.7	-0.7 ± 0.4		-4.9
Baffin Bay/Labrador Sea	0.4 ± 0.7		2.0	0.0 ± 1.1		0.1	2.0 ± 1.6		8.0	0.9 ± 1.3		7.2	-1.3 ± 0.6		-8.1
Gulf of St. Lawrence	0.9 ± 0.1	99	30.6	1.3 ± 0.4	99	16.6	1.5 ± 0.2	99	53.2	0.0 ± 0.0		0.0	0.9 ± 0.2	99	57.1
Greenland Sea	-2.4 ± 0.9	95	-9.8	-5.3 ± 1.5	99	-17.9	-1.9 ± 1.4		-7.2	-0.1 ± 1.3		-0.5	-2.1 ± 1.0	95	-10.9
Kara and Barents Seas	-1.5 ± 0.8		-5.5	0.7 ± 0.9		3.0	-0.2 ± 1.3		-0.8	-5.1 ± 2.0	95	-17.3	-1.4 ± 1.0		-5.5
Arctic Ocean	-1.4 ± 1.5		-2.9	-7.3 ± 1.9	99	-29.9	3.4 ± 2.5		11.8	2.0 ± 4.8		1.9	-3.9 ± 3.4		-8.8
Canadian Archipelago	0.7 ± 0.3	95	8.0	-1.3 ± 0.3	99	-25.7	1.3 ± 0.4	99	25.7	2.3 ± 0.5	99	14.1	0.3 ± 0.5		4.3

S indicates statistical significance and identifies those cases in which the null hypothesis of a 0 slope is rejected with a 95% confidence level (95) and a 99% confidence level (99), using a standard F test with 16 degrees of freedom.

show ice concentration increases (Plate 2a), the ice-free areas within the ice pack also increased (Table 3), a result, in this case, of the increased ice extent (Table 1) and hence the larger area over which the ice-free areas within the ice pack were summed.

In spring the largest-magnitude ice concentration trends are the negative trends in the eastern Barents Sea (Plate 2b), where they are also statistically significant (Plate 3b). These negative trends coincide with decreases in ice extent, ice area, and ice-free area within the ice pack (Tables 1-3), indicating a much reduced ice cover. In summer the largest-magnitude trends are the negative trends in the East Siberian Sea (70-76°N, 155-175°E) and in smaller areas north of Asia and the positive trends off the west coast of Greenland in northeastern Baffin Bay and in the eastern Beaufort Sea at about 130°W and 72°N (Plate 2c). In each of these cases the corresponding regions of section 3 are too large for ready comparisons, although, in general, there is a high significance level, with a ratio of trend to estimated standard deviation exceeding 3 (Plate 3c). In autumn also, the East Siberian Sea has negative ice concentration trends, northeastern Baffin Bay has positive ice concentration trends, and the eastern Beaufort Sea has positive ice concentration trends (Plate 2d), but in each of these cases the magnitude is reduced from that of the summer trends (Plate 2c). In autumn the highest-magnitude trends are the negative trends in the southern Kara Sea and off the coast of northern Alaska at about 165°W (Plate 2d). Once again, the highest-magnitude trend values exceed 3 estimated standard deviations (Plate 3d).

6. Discussion

As shown in section 3 and by *Cavalieri et al.* [1997], monthly averaged passive-microwave data from the SMMR and SSMI instruments over the period November 1978 through December 1996 reveal an overall negative trend in ice extents for the Northern Hemisphere. This result agrees with results previously found by *Johannessen et al.* [1995] and *Bjørgo et al.* [1997] for slightly shorter periods. As also shown in section 3, the negative trend comes regionally mostly from the Kara and Barents Seas and the next two major regional contributors to the negative slope are the Seas of Okhotsk and Japan and the Arctic Ocean. Lesser contributions come from the Greenland Sea, Hudson Bay, and the Canadian Archipelago (Table 1). The remaining three regions, the Bering Sea, Baffin Bay/Labrador Sea, and the Gulf of St. Lawrence, exhibit slight, positive trends over the SMMR/SSMI period, with the largest positive trend being for the region of Baffin Bay/Labrador Sea but the only statistically significant positive trend (at a 95% confidence level or above) being for the Gulf of St. Lawrence (Table 1).

For most regions and the total, changes from one year to another often far exceed the rate of change indicated in the long-term trend, and adjustment by a few years of the starting and/or ending times of the trend calculation would, in some instances, change the sign of the slope. Hence we caution against extrapolating the trend lines and slopes given here to times prior to the November 1978 start of the data set or subsequent to the December 1996 end of the data set. The results presented provide specific, quantified information about Arctic sea ice extents over an 18.2-year period, showing considerable regional and interannual variability but no trends that can be clearly identified as long-term climate trends appropriate for extrapolation beyond the 18.2 years. In fact, an analysis of Arctic sea ice fluctuations over the 25 years 1953-1977, prior to the SMMR/SSMI time period, reveals a slight (3140 km^2/yr) but statistically significant positive trend in 1953-1977 ice extents [*Walsh and Johnson*, 1979]. The negative trend (-34,000 km^2/yr) reported here for the yearly averages in the Northern Hemisphere as a whole over the 18-year period 1979-1996 is an order of magnitude greater than the 1953-1977 positive trend but is for a shorter period.

To confirm that the ice extent trends of Figures 1-10 and Table 1 are robust in terms of not being dramatically dependent on the choice of 15% as the ice concentration cutoff used in the definition of ice extent, the calculations were redone using 20% and then 30% as the ice concentration cutoff. (For instance, in the 20% case, ice extent is defined as the cumulative area of all grid cells, in the region of interest, having calculated sea ice concentrations of at least 20%.) Figure 14 presents the yearly average results for each region having statistical significance in the yearly averaged trend (Table 1) and additionally the seasonal results for the Northern Hemisphere totals. This selection is a good sampling of the results for all of the regions and seasons, showing the near but not perfect parallelism of the 15%, 20%, and 30% curves. In each case the sign of the slope of the line of linear least squares fit is the same, irrespective of which ice concentration cutoff is used; and although the magnitudes of the slopes are generally different for the different cutoffs, in each case the level of statistical significance (95%, 99%, or none) remains the same (Table 4). Furthermore, in all cases except one, the slopes of the 20% and 30% ice extents are within 1 standard deviation of the 15% ice extent slope.

The smaller percent interannual variability in the Northern Hemisphere total than in many of the regions (Figure 1a versus the regional monthly average plots) reflects the compensating changes that often occur, many times as a result of atmospheric pressure systems that tend to lessen ice coverage in one region while increasing it in another. Examples include the occasional out-of-phase nature of the ice coverages of the Bering Sea and the Sea of Okhotsk [*Cavalieri and Parkinson*, 1987] and of other pairs of adjacent seas separated by a geographical boundary. The particularly strong interannual variability found in the ice extents of the Greenland Sea and the Kara and Barents Seas (Figures 7a and 8a) is likely related to the influence of North Atlantic storm systems. In fact, the strongest winter cyclones in the north polar region tend to be over the Iceland and Norwegian Seas, with the highest cyclone frequencies being just south of Iceland and high frequencies also occurring between Svalbard and Scandinavia and over the Norwegian and Kara Seas [*Serreze et al.*, 1993]. Central cyclonic pressures in these regions are frequently below 970 mbar [*Serreze et al.*, 1993], generating winds that will, depending upon the precise positioning of the cyclone, sometimes decrease ice extents in the Greenland Sea by pushing the ice toward the Greenland coast and other times increase ice extents in the Greenland Sea by spreading ice southward. Similarly, they will sometimes decrease and sometimes increase the ice coverage in the Kara and Barents Seas. *Shuchman et al.* [1998] provide more details specifically for the Odden feature in the Greenland Sea ice cover, showing, through comparisons between ice and atmospheric data, the importance of temperature and wind conditions to the Odden growth, maintenance, and decay.

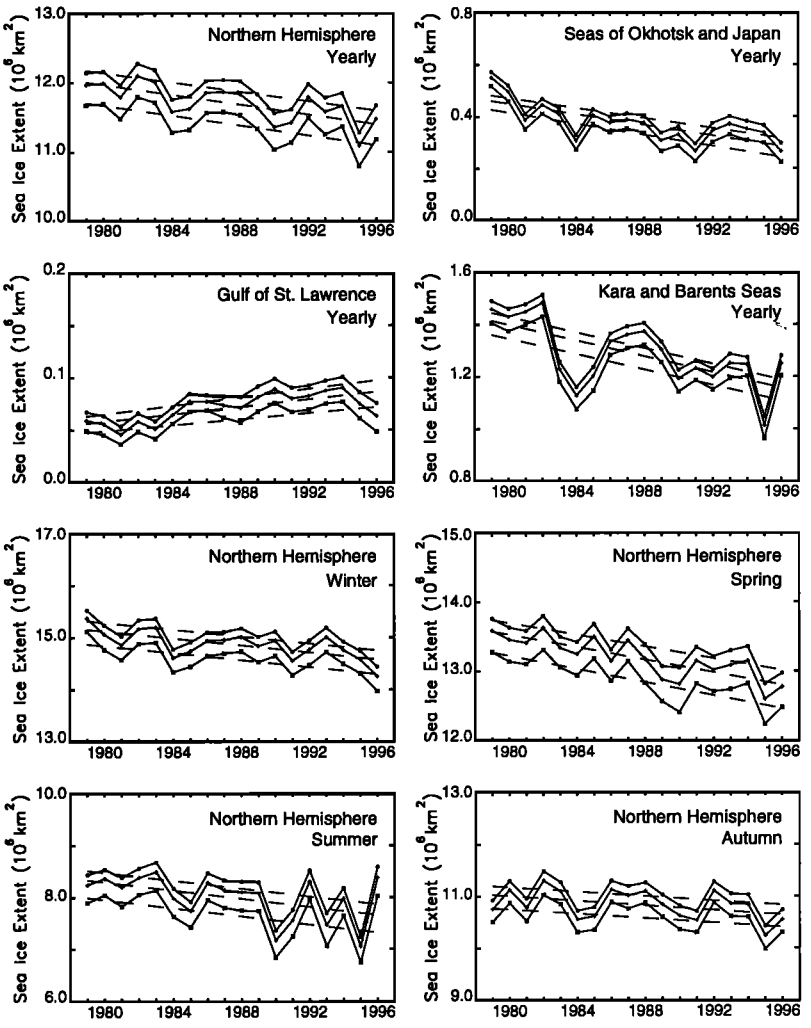

Figure 14. Selection of yearly and seasonal ice extent values and trend lines plotted for three choices of ice concentration cutoff used in the definition of ice extent. In each case the top curve uses a 15% ice concentration cutoff, as in Figures 1-10, whereas the middle curve uses a 20% cutoff and the bottom curve uses a 30% cutoff. Yearly values are plotted for the Northern Hemisphere, the Seas of Okhotsk and Japan, the Gulf of St. Lawrence, and the Kara and Barents Seas; and seasonal values are plotted for the Northern Hemisphere.

Table 4. Slopes, and Their Estimated Standard Deviations, of the Lines of Linear Least Squares Fit Through 1979-1996 Yearly Sea Ice Extents for Regions With Statistically Significant Yearly Slopes in Table 1 and Seasonal Sea Ice Extents for the Northern Hemisphere

Region	Type	15% Cutoff		20% Cutoff		30% Cutoff	
		10^3 km^2/yr	S	10^3 km^2/yr	S	10^3 km^2/yr	S
Northern Hemisphere	yearly	-34.0 ± 8.3	99	-35.6 ± 8.4	99	-35.8 ± 8.4	99
Seas of Okhotsk and Japan	yearly	-9.7 ± 2.3	99	-10.3 ± 2.3	99	-10.8 ± 2.3	99
Gulf of St. Lawrence	yearly	2.0 ± 0.4	99	1.8 ± 0.4	99	1.4 ± 0.5	99
Kara and Barents Seas	yearly	-15.2 ± 4.4	99	-15.2 ± 4.5	99	-14.9 ± 4.5	99
Northern Hemisphere	winter	-33.6 ± 9.2	99	-34.3 ± 9.2	99	-34.0 ± 9.2	99
Northern Hemisphere	spring	-42.8 ± 7.5	99	-45.5 ± 7.7	99	-47.6 ± 8.1	99
Northern Hemisphere	summer	-38.3 ± 17.6	95	-40.0 ± 17.5	95	-40.0 ± 17.3	95
Northern Hemisphere	autumn	-21.5 ± 11.9		-22.7 ± 12.0		-21.7 ± 12.2	

Slopes are provided for three choices (15%, 20%, and 30%) of ice concentration cutoff in the definition of ice extent. S indicates statistical significance and identifies those cases in which the null hypothesis of a 0 slope is rejected with a 95% confidence level (95) and a 99% confidence level (99), using a standard F test with 16 degrees of freedom.

The ice increases in Baffin Bay/Labrador Sea and the Gulf of St. Lawrence (Figures 5-6) contrasted with the decreases in the Greenland Sea, Kara and Barents Seas, and Arctic Ocean (Figures 7-9) are likely tied to the large-scale atmospheric patterns of the North Atlantic Oscillation. The NAO, calculated as the normalized atmospheric pressure at Lisbon, Portugal, minus that at Stykkisholmur, Iceland, has been above average since 1980, with a strong Azores High and, most importantly for the sea ice cover, a strong Icelandic Low [*Hurrell*, 1995; *Dickson et al.*, 1996]. The result includes strong southwesterlies across the North Atlantic, with anomalously high temperatures over northern Europe and Asia, and strong north winds over Baffin Bay and the Labrador Sea, with consequent anomalously low temperatures in those regions [*Hurrell*, 1995; *Hurrell and van Loon*, 1997]. In addition to an intensified Icelandic Low, atmospheric pressures have also decreased over the Arctic Ocean, as revealed from data of the Arctic Ocean Buoy Program for 1979-1994 [*Walsh et al.*, 1996]. This has decreased the anticyclonic wind forcing on the Arctic Ocean sea ice and decreased the atmospheric forcing of the Transpolar Drift Stream across the Arctic Basin, through Fram Strait, and into the Greenland Sea [*Walsh et al.*, 1996]. Decreased southward flow into the Greenland Sea is consistent with the decreasing sea ice extents found for the Greenland Sea (Figure 7, Table 1). The sea ice trends determined for these regions from the 1978-1996 SMMR and SSMI data (Figures 5-9, Table 1) can thus be viewed as a part of the larger-scale happenings within the climate system, in this case particularly the NAO in atmospheric pressures between Iceland and Portugal and the decreases in Arctic atmospheric pressures. The NAO influence also extends well below the ocean surface, with the rise in the NAO index since the 1960s being believed to have contributed to the decreasing deep convection in the Greenland Sea and the increasing deep convection in the Labrador Sea [*Dickson et al.*, 1996]. This, in turn, has led to warming of the deep water of the Greenland Sea and cooling of the deep water of the Labrador Sea [*Dickson et al.*, 1996].

On longer timescales many studies have found an expected negative correlation between sea ice coverage and atmospheric temperatures. For instance, such correlations were found by *Rogers* [1978] in the Beaufort Sea, by *Walsh and Johnson* [1979] for the Arctic as a whole, and by *Manak and Mysak* [1989] for the Beaufort Sea, Hudson Bay, and Baffin Bay/Labrador Sea. Using a 30-year record from 1961 to 1990, *Chapman and Walsh* [1993] found Arctic sea ice variations to be consistent with the corresponding air temperature changes, the latter showing an overall warming in the Arctic, although a cooling over Baffin Bay, the Labrador Sea, and the southern Greenland Sea (conducive to ice extent decreases in the Arctic and increases in Baffin Bay/Labrador Sea, as in Figures 5 and 9 and Table 1). Seasonally, the 1961-1990 warming was strongest in winter and spring, whereas the sea ice decreases were highest in spring and summer [*Chapman and Walsh*, 1993]. (Relatedly, the Intergovernmental Panel on Climate Change (IPCC) found warming from 1955-1974 to 1975-1994 over much of the Arctic periphery but cooling over Baffin Bay, the Labrador Sea, and the southern Greenland Sea [*Nicholls et al.*, 1996]. However, in a separate study an overall warming was not detectable in the lower troposphere over the Arctic Ocean over the period 1950-1990 [*Kahl et al.*, 1993]. Temperature data for the Arctic have been notoriously sparse, although improved data sets from 1979 onward are now being generated through combining buoy data from the International Arctic Buoy Program with ship reports and data from drifting ice stations and coastal weather stations [*Martin and Munoz*, 1997].) Looking more specifically at anomalous years, *Mysak et al.* [1996] find unusually heavy ice coverages in Hudson Bay, Baffin Bay, and the Labrador Sea in each of the three periods, 1972/1973, 1982/1983, and 1991/1992, with simultaneous strong North Atlantic Oscillation and El Niño-Southern Oscillation episodes, in each case finding a link with low surface air temperature anomalies lasting for several seasons. The heavy ice coverages are consistent with the finding by *Mysak* [1986] of low sea surface temperatures in the northwest North Atlantic during El Niño episodes. These specific cases show connections between the ice cover and other elements of the climate system. As the records lengthen, the connections should be further clarified and the climate system more fully understood.

Acknowledgments. We gratefully acknowledge Jamila Saleh of Raytheon STX for her help in the generation of the figures; Jamila and her colleagues Steve Fiegles and Mike Martino, also of Raytheon STX, for the processing of the data; and the National Snow and Ice Data Center (NSIDC) in Boulder, Colorado, for providing the SSMI radiances. We also thank two anonymous reviewers and JGR editors Ruth Preller and Mark Drinkwater for their time and effort and Leif Toudal Pedersen and John Walsh for excellent reviews and suggestions. This work was supported by NASA's Earth Observing System (EOS) program and by the Polar Programs at NASA Headquarters.

References

Aagaard, K., and E. C. Carmack, The role of sea ice and other fresh water in the Arctic circulation, *J. Geophys. Res.*, *94*(C10), 14,485-14,498, 1989.

Barry, R. G., M. C. Serreze, J. A. Maslanik, and R. H. Preller, The Arctic sea ice-climate system: Observations and modeling, *Rev. Geophys.*, *31*(4), 397-422, 1993.

Bjørgo, E., O. M. Johannessen, and M. W. Miles, Analysis of merged SMMR-SSMI time series of Arctic and Antarctic sea ice parameters 1978-1995, *Geophys. Res. Lett.*, *24*(4), 413-416, 1997.

Cavalieri, D. J., and C. L. Parkinson, On the relationship between atmospheric circulation and the fluctuations in the sea ice extents of the Bering and Okhotsk Seas, *J. Geophys. Res.*, *92*(C7), 7141-7162, 1987.

Cavalieri, D. J., P. Gloersen, C. L. Parkinson, J. C. Comiso, and H. J. Zwally, Observed hemispheric asymmetry in global sea ice changes, *Science*, *278*, 1104-1106, 1997.

Cavalieri, D. J., C. L. Parkinson, P. Gloersen, J. C. Comiso, and H. J. Zwally, Deriving long-term time series of sea ice cover from satellite passive-microwave multisensor data sets, *J. Geophys. Res.*, *104*, 15,803- 15,814, 1999.

Chapman, W. L., and J. E. Walsh, Recent variations of sea ice and air temperature in high latitudes, *Bull. Am. Meteorol. Soc.*, *74*(1), 33-47, 1993.

Comiso, J. C., and R. Kwok, Surface and radiative characteristics of the summer Arctic sea ice cover from multisensor satellite observations, *J. Geophys. Res.*, *101*(C12), 28,397-28,416, 1996.

Dickson, R., J. Lazier, J. Meincke, P. Rhines, and J. Swift, Long-term coordinated changes in the convective activity of the North Atlantic, *Prog. Oceanogr.*, *38*(3), 241-295, 1996.

Draper, N. R., and H. Smith, *Applied Regression Analysis*, 2nd ed., 709 pp., John Wiley, New York, 1981.

Gloersen, P., and W. J. Campbell, Recent variations in Arctic and Antarctic sea-ice covers, *Nature*, *352*, 33-36, 1991.

Gloersen, P., W. J. Campbell, D. J. Cavalieri, J. C. Comiso, C. L. Parkinson, and H. J. Zwally, Arctic and antarctic sea ice, 1978-1987: Satellite passive-microwave observations and analysis, *NASA SP-511*, 290 pp., 1992.

Gloersen, P., J. Yu, and E. Mollo-Christensen, Oscillatory behavior in Arctic sea ice concentrations, *J. Geophys. Res.*, *101*(C3), 6641-6650, 1996.

Gloersen, P., C. L. Parkinson, D. J. Cavalieri, J. C. Comiso, and H. J. Zwally, Spatial distribution of trends and seasonality in the hemispheric sea ice covers: 1978-1996, *J. Geophys. Res.*, this issue.

Häkkinen, S., An Arctic source for the Great Salinity Anomaly: A simulation for the Arctic ice-ocean system for 1955-1975, *J. Geophys. Res.*, *98*(C9), 16,397-16,410, 1993.

Hurrell, J. W., Decadal trends in the North Atlantic Oscillation: Regional temperatures and precipitation, *Science*, *269*, 676-679, 1995.

Hurrell, J. W., and H. van Loon, Decadal variations in climate associated with the North Atlantic Oscillation, *Clim. Change*, *36*(3), 301-326, 1997.

Johannessen, O. M., M. Miles, and E. Bjørgo, The Arctic's shrinking sea ice, *Nature*, *376*, 126-127, 1995.

Kahl, J. D., D. J. Charlevoix, N. A. Zaitseva, R. C. Schnell, and M. C. Serreze, Absence of evidence for greenhouse warming over the Arctic Ocean in the past 40 years, *Nature*, *361*, 335-337, 1993.

Manak, D. K., and L. A. Mysak, On the relationship between Arctic sea-ice anomalies and fluctuations in Northern Canadian air temperature and river discharge, *Atmos.-Ocean*, *27*(4), 682-691, 1989.

Martin, S., and E. A. Munoz, Properties of the Arctic 2-meter air temperature field for 1979 to the present derived from a new gridded dataset, *J. Clim.*, *10*, 1428-1440, 1997.

Maslanik, J. A., M. C. Serreze, and R. G. Barry, Recent decreases in Arctic summer ice cover and linkages to atmospheric circulation anomalies, *Geophys. Res. Lett.*, *23*(13), 1677-1680, 1996.

Massom, R., *Satellite Remote Sensing of Polar Regions*, 307 pp., Belhaven, London, 1991.

Mysak, L. A., El Niño, interannual variability and fisheries in the northeast Pacific Ocean, *Can. J. Fish. Aquat. Sci.*, *43*, 464-497, 1986.

Mysak, L. A., and S. B. Power, Sea-ice anomalies in the western Arctic and Greenland-Iceland Sea and their relation to an interdecadal climate cycle, *Climatol. Bull.*, *26*, 147-176, 1992.

Mysak, L. A., R. G. Ingram, J. Wang, and A. van der Baaren, The anomalous sea-ice extent in Hudson Bay, Baffin Bay and the Labrador Sea during three simultaneous NAO and ENSO episodes, *Atmos. Ocean*, *34*(2), 313-343, 1996.

National Snow and Ice Data Center (NSIDC), DMSP SSM/I brightness temperatures and sea ice concentration grids for the polar regions on CD-ROM user's guide, *Spec. Rep. 1*, Coop. Inst. for Res. in Environ. Sci., Univ. of Colo., Boulder, 1992.

Nicholls, N., G. V. Gruza, J. Jouzel, T. R. Karl, L. A. Ogallo, and D. E. Parker, Observed climate variability and change, in *Climate Change 1995: The Science of Climate Change*, edited by J. T. Houghton et al., pp.133-192, Cambridge Univ. Press, New York, 1996.

Parkinson, C. L., The impact of the Siberian High and Aleutian Low on the sea-ice cover of the Sea of Okhotsk, *Ann. Glaciol.*, *14*, 226-229, 1990.

Parkinson, C. L., Recent sea-ice advances in Baffin Bay/Davis Strait and retreats in the Bellingshausen Sea, *Ann. Glaciol.*, *21*, 348-352, 1995.

Parkinson, C. L., and D. J. Cavalieri, Arctic sea ice 1973-1987: Seasonal, regional, and interannual variability, *J. Geophys. Res.*, *94*(C10), 14,499-14,523, 1989.

Parkinson, C. L., J. C. Comiso, H. J. Zwally, D. J. Cavalieri, P. Gloersen, and W. J. Campbell, Arctic sea ice, 1973-1976: Satellite passive-microwave observations, *NASA SP-489*, 296 pp., 1987.

Pollard, J. H., *A Handbook of Numerical and Statistical Techniques*, 349 pp., Cambridge Univ. Press, New York, 1981.

Pritchard, R. S. (Ed.), *Sea Ice Processes and Models*, 474 pp., Univ. of Wash. Press, Seattle, 1980.

Robinson, D. A., K. F. Dewey, and R. R. Heim, Global snow cover monitoring: An update, *Bull. Am. Meteorol. Soc.*, *74*(9), 1689-1696, 1993.

Rogers, J. C., Meteorological factors affecting the interannual variability of summertime ice extent in the Beaufort Sea, *Mon. Weather Rev.*, *106*, 890-897, 1978.

Serreze, M. C., J. E. Box, R. G. Barry, and J. E. Walsh, Characteristics of Arctic synoptic activity, 1952-1989, *Meteorol. Atmos. Phys.*, *51*, 147-164, 1993.

Serreze, M. C., J. A. Maslanik, J. R. Key, and R. F. Kokaly, Diagnosis of the record minimum in Arctic sea ice area during 1990 and associated snow cover extremes, *Geophys. Res. Lett.*, *22*(16), 2183-2186, 1995.

Shuchman, R. A., E. G. Josberger, C. A. Russel, K. W. Fischer, O. M. Johannessen, J. Johannessen, and P. Gloersen, Greenland Sea Odden sea ice feature: Intra-annual and interannual variability, *J. Geophys. Res.*, *103*(C6), 12,709-12,724, 1998.

Taylor, J. R., *An Introduction to Error Analysis: The Study of Uncertainties in Physical Measurements*, 2nd ed., 327 pp., Univ. Sci. Books, Sausalito, Calif., 1997.

Toudal Pedersen, L., D. Low, H. Valeur, and P. Wadhams, Satellite observations of the Odden ice cover during the winter of 1995-1996, *Rep. DTU R 656*, 46 pp., Tech. Univ. of Denmark, Lyngby, 1997.

Wadhams, P., N. R. Davis, J. C. Comiso, R. Kutz, J. Crawford, G. Jackson, W. Krabill, C. B. Sear, R. Swift, and W. B. Tucker III, Concurrent remote sensing of Arctic sea ice from submarine and aircraft, *Int. J. Remote Sens.*, *12*(9), 1829-1840, 1991.

Walsh, J. E., and C. M. Johnson, An analysis of Arctic sea ice fluctuations, 1953-77, *J. Phys. Oceanogr.*, *9*(3), 580-591, 1979.

Walsh, J. E., W. L. Chapman, and T. L. Shy, Recent decrease of sea level pressure in the Central Arctic, *J. Clim.*, *9*, 480-486, 1996.

D. J. Cavalieri, J. C. Comiso, P. Gloersen, C. L. Parkinson, and H. J. Zwally, Oceans and Ice Branch, Code 971, NASA Goddard Space Flight Center, Greenbelt, MD 20771. (Claire.L.Parkinson.1@gsfc.nasa.gov)

(Received June 15, 1998; revised January 22, 1999;
accepted March 12, 1999.)